A Sensor-Based Controller for Homing of Underactuated AUVs

Pedro Batista, Carlos Silvestre, and Paulo Oliveira

IEEE Transactions on Robotics, vol. 25, no. 3, pp. 701-716, June 2009

https://doi.org/10.1109/TRO.2009.2014496

A Sensor Based Controller for Homing of Underactuated AUVs

Pedro Batista, *Student Member, IEEE,* Carlos Silvestre, *Member, IEEE,* and Paulo Oliveira, *Member, IEEE*

***Abstract*—A new sensor based homing integrated guidance and control law is presented to drive an underactuated autonomous underwater vehicle (AUV) towards a fixed target, in 3D, using the information provided by an Ultra-Short Baseline (USBL) positioning system. The guidance and control law is firstly derived using quaternions to express the vehicle's attitude kinematics, which are directly obtained from the time differences of arrival (TDOA) measured by the USBL sensor. The dynamics are then included resorting to backstepping techniques. The proposed Lyapunov-based control law yields global asymptotic stability (GAS) in the absence of external disturbances and is further extended, keeping the same properties, to the case where constant known ocean currents affect the dynamics of the vehicle. Finally, a globally exponentially stable (GES) nonlinear TDOA and range based observer is introduced to estimate the ocean current and uniform asymptotic stability is obtained for the overall closed-loop system. Simulations are presented illustrating the performance of the proposed solutions.**

***Index Terms*—mobile robots, underwater vehicles, underwater vehicle control, nonlinear systems, Lyapunov methods, position control, underwater acoustic arrays**

I. INTRODUCTION

ADVANCES in sensing devices, materials, and computational capabilities have provided the means to develop sophisticated underwater vehicles which nowadays display the capability to perform complex tasks in challenging, dangerous, and uncertain operation scenarios. In the last years several sophisticated Autonomous Underwater Vehicles (AUVs) and Remotely Operated Vehicles (ROVs) have been developed, endowing the scientific community with cutting-edge research tools supported in on-board complex mission and vehicle control systems, see [1], [2], and [3]. This paper presents the design and performance evaluation of a sensor-based integrated guidance and control law to drive an underactuated autonomous underwater vehicle towards a fixed target, in 3D, in the presence of unknown constant ocean currents.

The topic of navigation, guidance, and control of underwater vehicles has been subject of intensive research in the past decades, presenting numerous challenges that range from technical limitations, arising due to the particular nature of the surrounding oceanic environment, to theoretical problems, which exist even for fully actuated underwater vehicles. Indeed, while the control of fully actuated systems is generally fairly well understood, as evidenced by the large body of publications, see [4], [5], [6], and the references therein, for underwater vehicles there are still interesting questions springing from, e.g., the lack of coupled experimentally validated dynamic models or the inability to readily identify plant parameters, which exhibit, in general, strong nonlinear behaviors. To tackle the problem of stabilization of an underactuated vehicle a variety of solutions has been proposed in the literature, e.g., [7], [8], [9], and [10]. In [11] a solution to the problem of following a straight line is presented and in [12] a way-point tracking controller for an underactuated AUV is introduced. A position and attitude tracking controller was proposed in [13], whereas trajectory tracking solutions for underactuated underwater vehicles were presented in, e.g., [14] and [15]. The problem of path-following has also received much attention, see, e.g., [16] and [17]. It turns out that all the aforementioned references share a common approach: the vehicle position is computed in the inertial coordinate frame and the control laws are developed in the body frame. Therefore, the computation of the linear tracking error vector is heavily affected by errors in the estimates of the attitude of the vehicle. Sensor based control has been a hot topic in the field of computer vision where the so-called visual servoing techniques have been the subject of intensive research effort during the last years, see [18], and [19] for further information.

The main contribution of this paper is the design of a sensor-based integrated guidance and control law to drive an underactuated AUV towards a fixed target, in 3D, using the information provided by an Ultra-Short Baseline (USBL) positioning system. The solution to this problem, usually denominated as homing in the literature, is critical to the successful long-term autonomous operation of AUVs since it allows for the vehicle to approach a base station or support vessel, which often offer docking capabilities and permit the AUV to sleep, recharge its batteries, transfer data, and download new mission parameters. Once the vehicle is close enough to the base different strategies are required to safely lock the AUV in the dock. This last stage, usually denominated as docking in the literature, may vary significantly depending on the vehicle itself, the location, and the type of docking station. It also usually requires extra aiding sensors, e.g., optical or electromagnetic aiding sensors, see [20], [21], [22], and [23] for further details on this subject.

In this paper it is assumed that an acoustic transponder is installed on a predefined fixed position in the mission scenario, denominated as target in the sequel, and an Ultra-Short Baseline (USBL) sensor, composed by an array of hydrophones and an acoustic emitter, is rigidly mounted on the vehicle's nose, as depicted in Fig. 1. During the homing phase the USBL

This work was partially supported by Fundação para a Ciência e a Tecnologia (ISR/IST plurianual funding) through the POS_Conhecimento Program that includes FEDER funds and by the project MAYA of the AdI.

The work of P. Batista was supported by a PhD Student Scholarship from the POCTI Programme of FCT, SFRH/BD/24862/2005.

The authors are with the Institute for Systems and Robotics, Instituto Superior Técnico, Av. Rovisco Pais, 1049-001 Lisboa, Portugal. {pbatista,cjs,pjcro}@isr.ist.utl.pt

sensor interrogates the transponder and synchronizes, detects and records the time of arrival and time differences of arrival (TDOA) as measured by each receiver. This gives the vehicle the direction and range to the target, as opposed to single-range homing strategies, see [24], [25], and [26], where the vehicle describes particular trajectories to detect the position of the beacon or somehow overcome the lack of knowledge of its direction. The advantage of using the USBL is that it allows, without the use of extra external devices, the measurement of the target's direction, which makes possible the design of simpler control strategies that do not require the vehicle to describe particular trajectories. Moreover, in the presence of unknown constant ocean currents, this sensor will allow the development of a globally exponentially stable (GES) observer for this quantity. Other navigation solutions based on single range measurements are presented in [27] and based on the dynamics of the vehicle in [28]. Previous work developed by the authors can be found found in [29], where a globally asymptotically stable (GAS) homing strategy was proposed based directly on the TDOA provided by an USBL but the problem of ocean current estimation was not addressed. In [30] the authors have also proposed an ocean current estimation solution but the proof of stability for the overall system required the assumption of bounded velocities and acceleration which was, although mild from the practical point of view since the propulsion system of the AUV limits the available force and torque, quite restrictive from the theoretical point of view. Finally, in [31], the authors address the problem of USBL-based navigation. This present paper generalizes the results presented in [30].

The present paper is organized as follows. In Section II the homing problem is introduced and the dynamics of the AUV are briefly described, whereas the USBL model is presented in Section III. A Lyapunov-based guidance and control law is firstly derived, in Section IV, using quaternions to express the vehicle attitude kinematics, which are directly obtained from the USBL data. This control law is then extended to include the dynamics of the vehicle resorting to backstepping techniques and, in Section V, it is further extended to the case where known constant ocean currents affect the vehicle dynamics. Global asymptotic stability is achieved in both cases. Afterwards, a globally exponentially stable nonlinear TDOA and range based observer is proposed to estimate the ocean current and uniform asymptotic stability is guaranteed for the overall closed-loop system. Simulation results are presented and discussed in Section VI, and finally Section VII summarizes the main results of the paper.

Throughout the paper the symbol $\mathbf{0}_{n\times m}$ denotes an $n \times m$ matrix of zeros, $\mathbf{I}_n$ an identity matrix with dimension $n \times n$, and $\operatorname{diag}(\mathbf{A}_1, \ldots, \mathbf{A}_\mathrm{n})$ a block diagonal matrix. When the dimensions are omitted the matrices are assumed of appropriate dimensions. The minimum and maximum singular values of a matrix $\mathbf{X}$ are denoted by $\sigma_{min}(\mathbf{X})$ and $\sigma_{max}(\mathbf{X})$, respectively.

II. Problem statement

Let $\{I\}$ be an inertial coordinate frame and $\{B\}$ the body-fixed coordinate frame, whose origin is located at the center of mass of the vehicle (see [32] for a thorough discussion of the coordinate frame conventions). Consider $\mathbf{p} = [x,\ y,\ z]^T$ as the position of the origin of $\{B\}$, described in $\{I\}$, $\mathbf{v} = [u,\ v,\ w]^T$ the linear velocity of the vehicle relative to $\{I\}$, expressed in body-fixed coordinates, and $\boldsymbol{\omega} = [p,\ q,\ r]^T$ the angular velocity, also expressed in body-fixed coordinates. The vehicle linear motion kinematics can be written as

$$\dot{\mathbf{p}} = \mathbf{R}\mathbf{v}, \tag{1}$$

where $\mathbf{R} = {}^{I}_{B}\mathbf{R} = ({}^{B}_{I}\mathbf{R})^T$ is the rotation matrix from $\{B\}$ to $\{I\}$, verifying

$$\dot{\mathbf{R}} = \mathbf{R}\mathbf{S}(\boldsymbol{\omega}),$$

where $\mathbf{S}(\mathbf{x})$ is the skew-symmetric matrix such that $\mathbf{S}(\mathbf{x})\mathbf{y} = \mathbf{x} \times \mathbf{y}$, with $\times$ denoting the cross product. The vehicle's dynamic equations of motion can be written in a compact form as

$$\begin{cases} \mathbf{M}\dot{\mathbf{v}} = -\mathbf{S}(\boldsymbol{\omega})\mathbf{M}\mathbf{v} - \mathbf{D}_\mathbf{v}(\mathbf{v})\mathbf{v} - \mathbf{g}_\mathbf{v}(\mathbf{R}) + \mathbf{b}_\mathbf{v} u_\mathbf{v} \\ \mathbf{J}\dot{\boldsymbol{\omega}} = -\mathbf{S}(\mathbf{v})\mathbf{M}\mathbf{v} - \mathbf{S}(\boldsymbol{\omega})\mathbf{J}\boldsymbol{\omega} - \mathbf{D}_{\boldsymbol{\omega}}(\boldsymbol{\omega})\boldsymbol{\omega} - \mathbf{g}_{\boldsymbol{\omega}}(\mathbf{R}) + \mathbf{u}_{\boldsymbol{\omega}} \end{cases}, \tag{2}$$

where

- $\mathbf{M} = \operatorname{diag}\{m_u, m_v, m_w\}$ is a positive definite diagonal mass matrix;
- $\mathbf{J} = \operatorname{diag}\{J_{xx}, J_{yy}, J_{zz}\}$ is a positive definite inertia matrix;
- $u_\mathbf{v} = \tau_u$ is the force control input that acts along the x_B axis;
- $\mathbf{u}_{\boldsymbol{\omega}} = [\tau_p,\ \tau_q,\ \tau_r]^T$ is the vector of torque control inputs that affect the rotation of the vehicle about the x_B, y_B, and z_B axes, respectively;
- $\mathbf{D}_\mathbf{v}(\mathbf{v}) = \operatorname{diag}\{X_u + X_{|u|u}|u|, Y_v + Y_{|v|v}|v|, Z_w + Z_{|w|w}|w|\}$ is the positive definite matrix of the linear motion drag coefficients;
- $\mathbf{D}_{\boldsymbol{\omega}}(\boldsymbol{\omega}) = \operatorname{diag}\{K_p + K_{|p|p}|p|, M_q + M_{|q|q}|q|, N_r + N_{|r|r}|r|\}$ is the matrix of the rotational motion drag coefficients;
- $\mathbf{b}_\mathbf{v} = [1,\ 0,\ 0]^T$;
- $\mathbf{g}_\mathbf{v}(\mathbf{R}) = \mathbf{R}^T[0,\ 0,\ W - B]^T$ represents the gravitational and buoyancy effects, W and B respectively, on the vehicle's linear motion;
- $\mathbf{g}_{\boldsymbol{\omega}}(\mathbf{R}) = \mathbf{S}(\mathbf{r}_B)\mathbf{R}^T[0,\ 0,\ B]^T$ accounts for the effect of the center of buoyancy displacement relatively to the center of mass, $\mathbf{r}_B$, on the vehicle rotational motion.

The mass and inertia matrices are assumed diagonal for the sake of simplicity but extensions will be provided for general forms of these matrices. The vehicle is assumed neutrally buoyant, i.e., $W = B$, which results in $\mathbf{g}_\mathbf{v}(\mathbf{R}) = \mathbf{0}$.

The homing problem considered in this paper can be stated as follows:

Problem Statement. *Consider an underactuated AUV with kinematics and dynamics given by* (1) *and* (2)*, respectively. Assume that a target equipped with an acoustic transponder is placed in a fixed position. Design a sensor based integrated guidance and control law to drive the vehicle towards a well defined neighborhood of the target using the time differences of arrival and range to the target as measured by an USBL sensor installed on the AUV.*

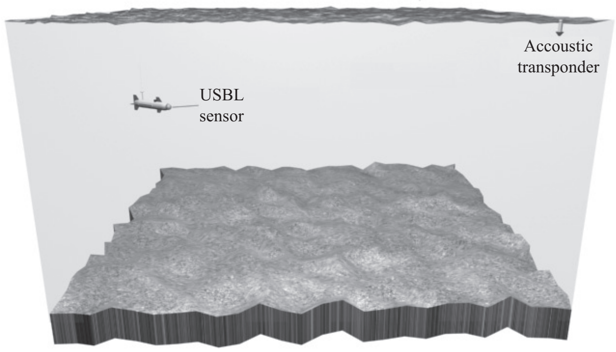

Fig. 1. Mission scenario

III. USBL MODEL

During the homing approach phase the vehicle is assumed to be far away from the acoustic emitter, that is, the distance from the vehicle to the target is much larger than the distance between any pair of receivers. Therefore, the plane-wave approximation is valid, see [33] for more details. Let $\mathbf{r}_i = [x_i,\ y_i,\ z_i]^T \in \mathbb{R}^3,\quad i = 1,\ 2,\ \ldots,\ N$, denote the positions of the N acoustic receivers installed on the USBL sensor and consider a plane-wave traveling along the opposite direction of the unit vector $\mathbf{d} = [d_x,\ d_y,\ d_z]^T$, corresponding to the direction of the target, as depicted in Fig. 2. Notice that both $\mathbf{r}_i$ and $\mathbf{d}$ are expressed in the body frame and the later corresponds to the direction of the target. Let t_i be the

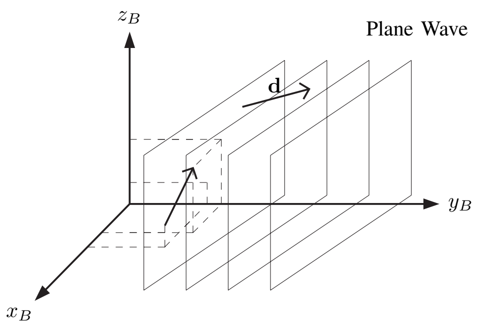

Fig. 2. Plane wave and the USBL system

time of arrival of the plane-wave at the i^{th} receiver and V_S the velocity of propagation of the sound in water, assumed to be constant and known. Then, assuming that the medium is homogeneous and neglecting the velocity of the vehicle, which is a reasonable assumption since $\|\mathbf{v}\| << V_S$, the time difference of arrival between receivers i and j satisfies

$$t_i - t_j = -\frac{d_x\,(x_i - x_j) + d_y\,(y_i - y_j) + d_z\,(z_i - z_j)}{V_S}. \quad (3)$$

Denote by $\Delta_1 = t_1 - t_2,\ \Delta_2 = t_1 - t_3,\ \ldots,\ \Delta_M = t_{N-1} - t_N$ all the possible combinations of TDOA, where $M = N\,(N-1)/2$, and let $\boldsymbol{\Delta} = [\Delta_1,\ \Delta_2,\ \cdots,\ \Delta_M]^T$. Define

$$\begin{aligned}
\mathbf{r}_x &:= [x_1 - x_2,\ x_1 - x_3,\ \cdots,\ x_{N-1} - x_N]^T,\\
\mathbf{r}_y &:= [y_1 - y_2,\ y_1 - y_3,\ \cdots,\ y_{N-1} - y_N]^T,\\
\mathbf{r}_z &:= [z_1 - z_2,\ z_1 - z_3,\ \cdots,\ z_{N-1} - z_N]^T,
\end{aligned}$$

and $\mathbf{H}_R \in \mathbb{R}^{M\times 3}$ as

$$\mathbf{H}_R = [\mathbf{r}_x,\ \mathbf{r}_y,\ \mathbf{r}_z].$$

Then, the generalization of (3) for all TDOA yields

$$\boldsymbol{\Delta} = -\frac{\mathbf{H}_R\mathbf{d}}{V_S}.$$

Define also

$$\mathbf{H}_Q := \frac{\mathbf{H}_R^T\mathbf{H}_R}{V_S} \in \mathbb{R}^{3\times 3},$$

which is assumed to be non-singular. This turns out to be a weak hypothesis as it is always true if, at least, 4 receivers are mounted in non-coplanar positions. In those conditions $\mathbf{H}_R$ has maximum rank and so does $\mathbf{H}_Q$. Then,

$$\mathbf{d} = -\mathbf{H}_Q^{-1}\mathbf{H}_R^T\boldsymbol{\Delta}, \quad (4)$$

which directly relates the direction of the target, as seen from the AUV, to the TDOA vector. The time derivative $\dot{\mathbf{d}}$ can be written as (see Appendix A for the calculations),

$$\dot{\mathbf{d}} = \mathbf{S}\,(\boldsymbol{\omega}_g)\,\mathbf{d}, \quad (5)$$

where $\boldsymbol{\omega}_g = -\boldsymbol{\omega} + \boldsymbol{\omega}_l$, with $\boldsymbol{\omega}_l = \mathbf{v}\times\mathbf{d}/\rho$. Notice that the first term represents the vehicle rotation velocity while the second term $\boldsymbol{\omega}_l$ denotes the induced rotation velocity due to the linear vehicle displacement. The range to the target, as measured by the USBL sensor, is represented by ρ.

IV. CONTROLLER DESIGN

In this section an integrated nonlinear closed-loop guidance and control law is derived for the homing problem stated earlier in Section II. Assuming that there are no ocean currents the idea behind the control strategy proposed here is to steer the vehicle directly towards the emitter. The synthesis of the guidance and control law resorts extensively to the Lyapunov's direct method and backstepping techniques whereas the kinematic error takes the form of a quaternion directly obtained from the TDOA provided by the USBL sensor.

To drive the vehicle with constant forward speed towards the target, define a first error variable as

$$z_1 := [1,\ 0,\ 0]\mathbf{v} - V_d,$$

where $V_d > 0$ is the desired vehicle velocity during the homing phase. When z_1 converges to zero, the surge speed converges to V_d. This single error variable is not sufficient to ensure that the vehicle is driven towards the target as the attitude of the vehicle is not controlled. Using (4), an attitude error can be defined in terms of a rotation matrix $\mathbf{R}_e$ that satisfies

$$\mathbf{R}_e[1, 0, 0]^T = -\mathbf{H}_Q^{-1}\mathbf{H}_R^T\boldsymbol{\Delta}. \quad (6)$$

When $\mathbf{R}_e$ is the identity matrix, the vehicle's x axis is aligned with the direction of the target. Equation (6) does not define uniquely a rotation matrix since one degree of freedom is left unconstrained with (6). The uniqueness of $\mathbf{R}_e$ is imposed by choosing an initial condition for the degree of freedom that is left unconstrained and by requiring it to preserve smoothness over time, which is always possible as the right side of (6) is continuous and continuously differentiable,

$$\dot{\mathbf{R}}_e = \mathbf{S}\left(\boldsymbol{\omega}_g\right)\dot{\mathbf{R}}_e. \tag{7}$$

In particular, let

$$\mathbf{R}_e\left(t_0\right) = \left[\begin{array}{ccc} -\mathbf{H}_Q^{-1}\mathbf{H}_R^T\boldsymbol{\Delta}\left(t_0\right) & \mathbf{d}_{20} & \mathbf{d}_{30}\end{array}\right]$$

be the initial rotation matrix $\mathbf{R}_e$. In order for smoothness to be preserved, it must be, from (7),

$$\left\{\begin{array}{l} \dot{\mathbf{d}}_2(t) = \mathbf{S}\left(\boldsymbol{\omega}_g\right)\dot{\mathbf{d}}_2(t) \\ \mathbf{d}_2\left(t_0\right) = \mathbf{d}_{20}\end{array}\right. ,$$

which provides the evolution of the degree of freedom that is left unconstrained by (6). To preserve orthogonality, particularly in the presence of measurement noise, one easy and computationally efficient solution is to compute the unit vector along the projection of $\mathbf{d}_2(t)$ on the plane orthogonal to $\mathbf{H}_Q^{-1}\mathbf{H}_R^T\boldsymbol{\Delta}(t)$, denoted by $\mathbf{d}_2^{\perp}(t)$, and then write

$$\mathbf{R}_e\left(t\right) = \left[-\mathbf{H}_Q^{-1}\mathbf{H}_R^T\boldsymbol{\Delta}(t) \;\; \mathbf{d}_2^{\perp}(t) \;\; \left[-\mathbf{H}_Q^{-1}\mathbf{H}_R^T\boldsymbol{\Delta}(t)\right]\times\left[\mathbf{d}_2^{\perp}(t)\right]\right].$$

Expressing $\mathbf{R}_e$ as $\mathbf{R}_e(\overline{q})$, where $\overline{q}$ is a unit quaternion corresponding to the same rotation, then the direction of the target is aligned with the body-fixed frame x axis when $\overline{q} = \pm(1,0,0,0)$. Define $\mathbf{q} = [q_0, \mathbf{q}_v^T]^T$ as the vector representation of $\overline{q}$, where q_0 and $\mathbf{q}_v$ are the so-called scalar and vector parts, respectively. It is now possible to define two new error variables to represent the attitude error,

$$z_2 := q_0 - 1 \tag{8}$$

and

$$\mathbf{z}_3 := \mathbf{q}_v. \tag{9}$$

Driving z_1, z_2, and $\mathbf{z}_3$ to zero is still insufficient to ensure the correct behavior of the vehicle during the homing phase as the sway and heave velocities are left free. However, it will be shown that, with the control law based upon these three error variables, the sway and heave velocities will also converge to zero, which completes a set of sufficient conditions to drive the vehicle towards the target. The quaternion dynamics are given by (see Appendix B for the calculations and see [34] for further details)

$$\dot{\mathbf{q}} = \frac{1}{2}\mathbf{D}(\boldsymbol{\omega}_g)\mathbf{q}, \tag{10}$$

where

$$\mathbf{D}(\boldsymbol{\omega}_g) = \left[\begin{array}{cc} 0 & -\boldsymbol{\omega}_g^T \\ \boldsymbol{\omega}_g & \mathbf{S}(\boldsymbol{\omega}_g)\end{array}\right].$$

To synthesize the control law, consider the Lyapunov function

$$V_1 := \frac{1}{2}z_1^2 + z_2^2 + \mathbf{z}_3^T\mathbf{z}_3.$$

The time derivative $\dot{V}_1$ can be written as (see Appendix C for the calculations)

$$\begin{aligned}\dot{V}_1 \;\; = \;\; & z_1\left([1,\,0,\,0]\mathbf{M}^{-1}\mathbf{b}_{\mathbf{v}}u_{\mathbf{v}} - [1,\,0,\,0]\mathbf{M}^{-1}\left[\mathbf{S}(\boldsymbol{\omega})\mathbf{M}\mathbf{v}\right.\right. \\ & \left.\left. +\mathbf{D}_{\mathbf{v}}(\mathbf{v})\mathbf{v}\right]\right) + \mathbf{z}_3^T\left(-\boldsymbol{\omega} + \boldsymbol{\omega}_l\right).\end{aligned}$$

Setting $u_{\mathbf{v}}$ as

$$u_{\mathbf{v}} = \frac{[1,\,0,\,0]\mathbf{M}^{-1}\left[\mathbf{S}(\boldsymbol{\omega})\mathbf{M}\mathbf{v} + \mathbf{D}_{\mathbf{v}}(\mathbf{v})\mathbf{v}\right] - k_1 z_1}{[1,\,0,\,0]\mathbf{M}^{-1}\mathbf{b}_{\mathbf{v}}}, \tag{11}$$

where k_1 is a positive scalar control gain, and $\boldsymbol{\omega} = \boldsymbol{\omega}_d$, with

$$\boldsymbol{\omega}_d := \mathbf{K}_2\mathbf{z}_3 + \boldsymbol{\omega}_l,$$

where $\mathbf{K}_2$ is a symmetric positive definite control gain matrix, the time derivative $\dot{V}_1$ becomes $\dot{V}_1 = -k_1 z_1^2 - \mathbf{z}_3^T\mathbf{K}_2\mathbf{z}_3$, which is strictly non-positive.

Although $u_{\mathbf{v}}$ is an actual control input, the same cannot be said about $\boldsymbol{\omega}$, which was regarded here as a virtual control input. Following the standard backstepping technique [35], define a fourth error variable

$$\mathbf{z}_4 := \boldsymbol{\omega} - \boldsymbol{\omega}_d \tag{12}$$

and the augmented Lyapunov function

$$V_2 := V_1 + \frac{1}{2}\mathbf{z}_4^T\mathbf{z}_4 = \frac{1}{2}z_1^2 + z_2^2 + \mathbf{z}_3^T\mathbf{z}_3 + \frac{1}{2}\mathbf{z}_4^T\mathbf{z}_4.$$

The time derivative of V_2 can be written as (see Appendix D for the calculations)

$$\begin{aligned}\dot{V}_2 \; = \; & -k_1 z_1^2 - \mathbf{z}_3^T\mathbf{K}_2\mathbf{z}_3 + \mathbf{z}_4^T\left(\mathbf{J}^{-1}\left[-\mathbf{S}(\mathbf{v})\mathbf{M}\mathbf{v} - \mathbf{S}(\boldsymbol{\omega})\mathbf{J}\boldsymbol{\omega}\right.\right. \\ & \left.\left. -\mathbf{D}_{\boldsymbol{\omega}}(\boldsymbol{\omega})\boldsymbol{\omega} - \mathbf{g}_{\boldsymbol{\omega}}(\mathbf{R}) + \mathbf{u}_{\boldsymbol{\omega}}\right] - \dot{\boldsymbol{\omega}}_d - \mathbf{z}_3\right).\end{aligned}$$

Now, setting

$$\begin{aligned}\mathbf{u}_{\boldsymbol{\omega}} \;\; = \;\; & \mathbf{S}(\mathbf{v})\mathbf{M}\mathbf{v} + \mathbf{S}(\boldsymbol{\omega})\mathbf{J}\boldsymbol{\omega} + \mathbf{D}_{\boldsymbol{\omega}}(\boldsymbol{\omega})\boldsymbol{\omega} + \mathbf{g}_{\boldsymbol{\omega}}(\mathbf{R}) \\ & +\mathbf{J}\left(\dot{\boldsymbol{\omega}}_d + \mathbf{z}_3 - \mathbf{K}_3\mathbf{z}_4\right),\end{aligned} \tag{13}$$

where $\mathbf{K}_3$ is a positive definite control gain matrix, finally yields $\dot{V}_2 = -k_1 z_1^2 - \mathbf{z}_3^T\mathbf{K}_2\mathbf{z}_3 - \mathbf{z}_4^T\mathbf{K}_3\mathbf{z}_4$. The time derivative $\dot{\boldsymbol{\omega}}_d$ is not presented here for the sake of simplicity.

Remark 1: Although during the synthesis of the control law four error variables have been defined, it is important to notice that it is not really necessary that z_2 converges to zero. Indeed, when $\mathbf{z}_3$ converges to zero, it follows that

$$\lim_{\mathbf{z}_3\to\mathbf{0}} z_2 = \pm 1,$$

or, in other words,

$$\lim_{\mathbf{z}_3\to\mathbf{0}} \overline{q} = \pm(1,0,0,0).$$

However, both $\overline{q} = (1,0,0,0)$ and $\overline{q} = -(1,0,0,0)$ correspond to $\mathbf{R}_e \to \mathbf{I}$, as intended.

The following theorem is the main result of this section.

Theorem 1: Consider a vehicle with kinematics and dynamics given by equations (1) and (2), respectively, moving in the absence of ocean currents and suppose the homing problem stated in Section II defined outside a ball of radius R_{min} and centered at the target's position. Further assume that

$$R_{min} > \frac{m_u}{\min\left\{Y_v, Z_w\right\}}V_d. \tag{14}$$

Then, with the control law (11)-(13), the equilibrium point $\mathbf{z} = \left[z_1, \mathbf{z}_3^T, \mathbf{z}_4^T\right]^T = \mathbf{0}$ is globally asymptotically stable and the sway and heave velocities converge to zero, thus solving globally the homing problem stated in Section II.

Proof: With the control law (11)-(13), the closed-loop error dynamics can be written as (see Appendix E for the calculations)

$$\begin{cases} \dot{z}_1 = -k_1 z_1 \\ \dot{z}_2 = \frac{1}{2}\left(\mathbf{z}_3^T \mathbf{K}_2 \mathbf{z}_3 + \mathbf{z}_3^T \mathbf{z}_4\right) \\ \dot{\mathbf{z}}_3 = -\frac{1}{2}\left[\left(z_2+1\right)\left(\mathbf{K}_2\mathbf{z}_3 + \mathbf{z}_4\right) + \mathbf{S}\left(\mathbf{K}_2\mathbf{z}_3 + \mathbf{z}_4\right)\mathbf{z}_3\right] \\ \dot{\mathbf{z}}_4 = \mathbf{z}_3 - \mathbf{K}_3\mathbf{z}_4 \end{cases},$$

which is an autonomous nonlinear system. The Lyapunov function V_2 is, by construction, continuous, radially unbounded, and positive definite. With the control law (11)-(13), the time derivative $\dot{V}_2$ results in

$$\dot{V}_2 = -k_1 z_1^2 - \mathbf{z}_3^T \mathbf{K}_2 \mathbf{z}_3 - \mathbf{z}_4^T \mathbf{K}_3 \mathbf{z}_4, \tag{15}$$

which is negative semi-definite. Therefore, V_2 is nonincreasing along all state trajectories, which remain bounded for all time. Moreover, V_2 approaches its own limit. Resorting to LaSalle's Theorem, it follows from (15) that z_1, $\mathbf{z}_3$ and $\mathbf{z}_4$ converge to zero [34]. Therefore, the x axis of the vehicle aligns itself with the desired direction. To complete the stability analysis all that is left to do is to show that the sway and heave velocities also converge to zero. Expanding the dynamics of the sway and heave velocities as in (2) yields

$$\begin{cases} \dot{v} = -\frac{Y_v + Y_{|v|v}|v|}{m_v} v + \frac{m_w}{m_v} p w - \frac{m_u}{m_v} u r \\ \dot{w} = -\frac{Z_w + Z_{|w|w}|w|}{m_w} w - \frac{m_v}{m_w} p v + \frac{m_u}{m_w} u q \end{cases}.$$

Now, after a few straightforward computations, it is possible to conclude that, when $\mathbf{z}$ converges to zero, the angular velocity converges to (see Appendix F for the proof)

$$\lim_{\mathbf{z}\to\mathbf{0}} \boldsymbol{\omega} = \frac{1}{\rho}\left[0, w, -v\right]^T.$$

On the other hand, when z_1 converges to zero, u converges to V_d. Thus, when $\mathbf{z}$ converges to zero, the dynamics of the sway and heave velocities can be written as the Linear Time Varying System (LTVS) driven by a vanishing disturbance $\mathbf{d}(t)$

$$\begin{bmatrix} \dot{v} \\ \dot{w} \end{bmatrix} = \mathbf{A}(t)\begin{bmatrix} v \\ w \end{bmatrix} + \mathbf{d}(t), \tag{16}$$

where

$$\mathbf{A}(t) = \begin{bmatrix} -\frac{Y_v + Y_{|v|v}|v| - \frac{m_u}{\rho} V_d}{m_v} & \frac{m_w}{m_v} p \\ -\frac{m_v}{m_w} p & -\frac{Z_w + Z_{|w|w}|w| - \frac{m_u}{\rho} V_d}{m_w} \end{bmatrix}.$$

Now, due to the fact that p also converges to zero and using (14), there exists t_0 such that for all $t > t_0$ the eigenvalues of the symmetric matrix $\mathbf{E}(t) = \frac{1}{2}\left[\mathbf{A}(t) + \mathbf{A}^T(t)\right]$, which are all real, remain strictly in the left-half complex plane. Thus, the LTVS (16) is asymptotically stable, which concludes the proof. ■

V. Control in the Presence of Ocean Currents

In this section the results from the previous section are generalized for the case where constant ocean currents are present. Firstly, the integrated guidance and control law synthesized in the previous section is modified assuming that the ocean current is known. Afterwards, a globally asymptotically stable observer that relies on the information provided by the sensors already installed on-board is proposed. Finally, the stability of the complete closed-loop system is addressed.

A. Controller Design

Consider that the vehicle is moving with velocity relative to the water $\mathbf{v}_r$ in the presence of an ocean current with velocity $\mathbf{v}_c$, both expressed in body-fixed coordinates. It is further assumed that the current velocity is constant in the inertial frame. The dynamics of the vehicle can then be rewritten as

$$\begin{cases} \mathbf{M}\dot{\mathbf{v}}_r = -\mathbf{S}(\boldsymbol{\omega})\mathbf{M}\mathbf{v}_r - \mathbf{D}_{v_r}(\mathbf{v}_r)\mathbf{v}_r + \mathbf{b}_\mathbf{v} u_\mathbf{v} \\ \mathbf{J}\dot{\boldsymbol{\omega}} = -\mathbf{S}(\mathbf{v}_r)\mathbf{M}\mathbf{v}_r - \mathbf{S}(\boldsymbol{\omega})\mathbf{J}\boldsymbol{\omega} - \mathbf{D}_\omega(\boldsymbol{\omega})\boldsymbol{\omega} - \mathbf{g}_\omega(\mathbf{R}) + \mathbf{u}_\boldsymbol{\omega} \end{cases} \tag{17}$$

and the vehicle's velocity relative to the inertial frame, expressed in body-fixed coordinates, is $\mathbf{v} = \mathbf{v}_r + \mathbf{v}_c$.

In this new mission scenario the control strategy synthesized in Section IV cannot be directly used, as the new control objective is to align the velocity of the vehicle relative to the inertial frame with the target's direction instead of the x axis of the vehicle. However, if the attitude error could be expressed as in Section IV, a similar control law could perhaps be used.

Consider the vehicle reference relative velocity $\mathbf{v}_R := [V_d, 0, 0]^T$, expressed in $\{B\}$. The error variable z_1, which accounts for the surge speed, is naturally modified to $z_1 := [1,\ 0,\ 0]\mathbf{v}_r - V_d$. Redefining the quaternion error $\overline{q}$ to correctly express the new attitude error, the error variables z_2 and $\mathbf{z}_3$ may remain unchanged. In order to do so, define a new coordinate system $\{E\}$ based on the direction of the emitter as follows: let the x axis of $\{E\}$ have direction $\mathbf{d}$, the y axis the direction of $\mathbf{i}_x \times \mathbf{d}$, where $\mathbf{i}_x = [1, 0, 0]^T$, and the z axis have the direction of $\mathbf{d} \times (\mathbf{i}_x \times \mathbf{d})$, all expressed in the body-fixed frame. The rotation matrix from $\{E\}$ to $\{B\}$ is given by

$$\begin{cases} {}^B_E\mathbf{R} = \left[\ \mathbf{d} \ \middle|\ \frac{\mathbf{i}_x \times \mathbf{d}}{\|\mathbf{i}_x \times \mathbf{d}\|} \ \middle|\ \frac{\mathbf{d}\times(\mathbf{i}_x\times\mathbf{d})}{\|\mathbf{d}\times(\mathbf{i}_x\times\mathbf{d})\|}\ \right], \mathbf{d}^T\mathbf{i}_x \neq \pm 1 \\ {}^B_E\mathbf{R} = \mathbf{I},\ \mathbf{d} = \mathbf{i}_x \\ {}^B_E\mathbf{R} = \mathrm{diag}\{-1, 1, -1\}, \mathbf{d} = -\mathbf{i}_x \end{cases}, \tag{18}$$

where $\mathbf{d}$, using (4), is directly obtained from the TDOA provided by the USBL sensor. Notice that, in the coordinate system $\{E\}$, the target's direction $\mathbf{d}$ is, by construction,

$$^E(\mathbf{d}) = [1,\ 0,\ 0]^T. \tag{19}$$

Denote by $^E\left(\mathbf{v}_r^O\right)$ the velocity of the vehicle relative to the water, expressed in $\{E\}$, when the vehicle is moving directly towards the target with speed V_d and no lateral velocity. Then, the relationship

$$\frac{^E\left(\mathbf{v}_r^O\right) + {}^E(\mathbf{v}_c)}{\|\,^E\left(\mathbf{v}_r^O\right) + {}^E(\mathbf{v}_c)\|} = {}^E(\mathbf{d}) \tag{20}$$

is satisfied. Using (19), it is straightforward to conclude that

$$\begin{bmatrix} 0 & 1 & 0 \\ 0 & 0 & 1 \end{bmatrix} {}^E\left(\mathbf{v}_r^O\right) = -\begin{bmatrix} 0 & 1 & 0 \\ 0 & 0 & 1 \end{bmatrix} {}^E(\mathbf{v}_c).$$

Figure 3 depicts an equivalent 2D version of the new coordinate frame $\{E\}$ and its relation with the several variables at hand.

Since $\|\,^E\left(\mathbf{v}_r^O\right)\| = V_d$, there are only two possible values left for the first component of $^E\left(\mathbf{v}_r^O\right)$. However, this component can be shown to be always positive (the proof is presented in Appendix G) under the reasonable assumption that $V_d > V_c$. In fact, if this assumption is not satisfied, it can be impossible for the vehicle to approach the target as its relative velocity

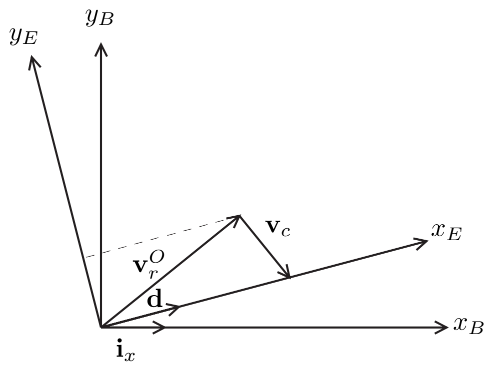

Fig. 3. Coordinate frames {E} and {B}

may be insufficient to counteract the ocean current. Thus, the signal ambiguity is solved and ${}^{E}\left(\mathbf{v}_r^O\right)$ uniquely defined. Now, an error definition equivalent to (6) can be written as

$$\mathbf{R}_e[V_d, 0, 0]^T := \mathbf{v}_r^O. \tag{21}$$

The same control strategy as in Section IV can be applied with minor changes in the control law: the relative velocity is now used to feed the control law $u_{\mathbf{v}}$ and the attitude error quaternion is obtained from (21). The induced rotation $\boldsymbol{\omega}_l$ also changes but is omitted here for the sake of simplicity (the expression of $\boldsymbol{\omega}_l$ is presented in Appendix H). The control law is now given by

$$u_{\mathbf{v}} = \frac{[1,\,0,\,0]\mathbf{M}^{-1}\left[\mathbf{S}(\boldsymbol{\omega})\mathbf{M}\mathbf{v}_r + \mathbf{D}_{v_r}(\mathbf{v}_r)\right] - k_1 z_1}{[1,\,0,\,0]\mathbf{M}^{-1}\mathbf{b}_{\mathbf{v}}} \tag{22}$$

and

$$\begin{aligned}\mathbf{u}_{\boldsymbol{\omega}} \;=\;& \mathbf{S}(\mathbf{v}_r)\mathbf{M}\mathbf{v}_r + \mathbf{S}(\boldsymbol{\omega})\mathbf{J}\boldsymbol{\omega} + \mathbf{D}_{\boldsymbol{\omega}}(\boldsymbol{\omega})\boldsymbol{\omega} + \mathbf{g}_{\boldsymbol{\omega}}(\mathbf{R}) \\ & + \mathbf{J}\left(\dot{\boldsymbol{\omega}}_d + \mathbf{z}_3 - \mathbf{K}_3\mathbf{z}_4\right).\end{aligned} \tag{23}$$

Global asymptotic stability is achieved (the proof is presented in Appendix I), as in Section IV, for

$$R_{min} > \frac{2m_u}{\min\{Y_v, Z_w\}} V_d. \tag{24}$$

B. A Globally Exponentially Stable Ocean Current Observer

In the previous section it was assumed that the velocity of the ocean current was known, which is perfectly feasible using an extra sensor, e.g., a Doppler velocity log when the vehicle is close to the seabed. However, when the vehicle is far from the sea bottom its inertial velocity is no longer available on-board and therefore an alternative solution must be adopted. In this section a nonlinear observer that makes use of the TDOA and target range measurements provided by the USBL sensor and the water relative velocity supplied by a Doppler velocity log is proposed and its stability analyzed.

The position of the target expressed in the body-fixed frame can be obtained directly from the USBL data. Using (4), it can be written as

$$\mathbf{e} = -\rho \mathbf{H}_Q^{-1}\mathbf{H}_R^T \boldsymbol{\Delta}. \tag{25}$$

As the emitter is fixed in the inertial frame, the time derivative of its position expressed in the body-fixed frame is given by

$$\dot{\mathbf{e}} = -\mathbf{v}_r - \mathbf{v}_c - \mathbf{S}(\boldsymbol{\omega})\mathbf{e}.$$

Because the current is assumed to be constant (in the inertial frame), the time derivative of the current expressed in the body-fixed frame simply results in

$$\dot{\mathbf{v}}_c = -\mathbf{S}(\boldsymbol{\omega})\mathbf{v}_c.$$

A globally exponentially stable observer for the water velocity expressed in the body frame is presented in the following theorem.

Theorem 2: Consider the observer in the body-fixed coordinate frame given by

$$\left\{\begin{array}{l}\dot{\hat{\mathbf{e}}} = -\mathbf{v}_r - \hat{\mathbf{v}}_c - \mathbf{S}(\boldsymbol{\omega})\mathbf{e} + \left[\mathbf{S}(\boldsymbol{\omega}) + k_{obs}\mathbf{I}\right](\mathbf{e} - \hat{\mathbf{e}}) \\ \dot{\hat{\mathbf{v}}}_c = -\mathbf{S}(\boldsymbol{\omega})\hat{\mathbf{v}}_c - (\mathbf{e} - \hat{\mathbf{e}})\end{array}\right., \tag{26}$$

where $\hat{\mathbf{e}}$ is the estimate of the emitter's position, $\mathbf{e}$ is the observed variable, given by (25), $\hat{\mathbf{v}}_c$ is the estimate of the velocity of the current, all expressed in the body-fixed frame, and $k_{obs} > 0$ is an observer gain. Then, the estimation errors

$$\left\{\begin{array}{l}\tilde{\mathbf{e}} = \mathbf{e} - \hat{\mathbf{e}} \\ \tilde{\mathbf{v}}_c = \mathbf{v}_c - \hat{\mathbf{v}}_c\end{array}\right.$$

converge globally exponentially fast to zero.

Proof: The time derivatives of the errors $\tilde{\mathbf{e}}$ and $\tilde{\mathbf{v}}_c$ can be written as

$$\left\{\begin{array}{l}\dot{\tilde{\mathbf{e}}} = -\tilde{\mathbf{v}}_c - \left[\mathbf{S}(\boldsymbol{\omega}) + k_{obs}\mathbf{I}\right]\tilde{\mathbf{e}} \\ \dot{\tilde{\mathbf{v}}}_c = -\mathbf{S}(\boldsymbol{\omega})\tilde{\mathbf{v}}_c + \tilde{\mathbf{e}}\end{array}\right.. \tag{27}$$

Consider the global diffeomorphic coordinate transformation $\mathbf{z}_{obs} = \mathbf{T}(\mathbf{R})[\tilde{\mathbf{e}}^T, \tilde{\mathbf{v}}_c^T]^T$, where

$$\mathbf{T}(\mathbf{R}) = \left[\begin{array}{c|c}\mathbf{R} & \mathbf{0}_{3\times 3} \\ \hline \mathbf{0}_{3\times 3} & \mathbf{R}\end{array}\right],$$

After a few straightforward computations the following linear time invariant system is obtained,

$$\dot{\mathbf{z}}_{obs} = \left[\begin{array}{cc}-k_{obs}\mathbf{I}_3 & -\mathbf{I}_3 \\ \mathbf{I}_3 & \mathbf{0}_{3\times 3}\end{array}\right]\mathbf{z}_{obs},$$

which is exponentially stable for $k_{obs} > 0$, from which follows that the origin of (27) is globally exponentially stable. ■

Remark 2: Constant currents are a common assumption when designing ocean current observers. Nevertheless, it is important to notice that the proposed observer is GES and its convergence rate may be tuned using the observer gain k_{obs}. For slowly time-varying ocean currents, if k_{obs} is chosen such that the observer has a small time constant when compared to the rate of change of the ocean currents, it should provide adequate tracking of the ocean current velocity.

C. Closed-loop stability analysis

The presence of an observer to estimate the velocity of the ocean current introduces an error $\tilde{\mathbf{u}}_{\boldsymbol{\omega}} = \hat{\mathbf{u}}_{\boldsymbol{\omega}} - \mathbf{u}_{\boldsymbol{\omega}}$ in the control input $\mathbf{u}_{\boldsymbol{\omega}}$. Indeed, due to the velocity error $\tilde{\mathbf{v}}_c$, the control law (23) is now replaced by

$$\begin{aligned}\hat{\mathbf{u}}_{\boldsymbol{\omega}} \;=\;& \mathbf{S}(\mathbf{v}_r)\mathbf{M}\mathbf{v}_r + \mathbf{S}(\boldsymbol{\omega})\mathbf{J}\boldsymbol{\omega} + \mathbf{D}_{\boldsymbol{\omega}}(\boldsymbol{\omega})\boldsymbol{\omega} + \mathbf{g}_{\boldsymbol{\omega}}(\mathbf{R}) \\ & + \mathbf{J}\left(\hat{\dot{\boldsymbol{\omega}}}_d + \hat{\mathbf{z}}_3 - \mathbf{K}_3\hat{\mathbf{z}}_4\right),\end{aligned} \tag{28}$$

where $\hat{\dot{\boldsymbol{\omega}}}_d$, $\hat{\mathbf{z}}_3$, and $\hat{\mathbf{z}}_4$ are the estimates of $\dot{\boldsymbol{\omega}}_d$, $\mathbf{z}_3$, and $\mathbf{z}_4$, respectively. Notice that the velocity error appears both directly and indirectly, as some of the variables depend implicitly on the velocity of the current, namely $\mathbf{v}_r^O$ and the quaternion $\mathbf{q}$. However, the maps from $\tilde{\mathbf{v}}_c$ to $\tilde{\mathbf{v}}_r^O$ and $\tilde{\mathbf{q}}$ are smooth and the origin of $\tilde{\mathbf{v}}_c$ is mapped onto the origin in both cases.

The stability of the overall closed-loop system is addressed in the following theorem.

Theorem 3: Consider the nonlinear system consisting of a vehicle with kinematics and dynamics given by equations (1) and (17), respectively, the current observer (26), and the control law given by (22) and (28). Suppose the homing problem as stated in Theorem 1 under Assumtion (24). Then, the equilibrium point $\mathbf{z} = [z_1, \mathbf{z}_3^T, \mathbf{z}_4^T]^T = \mathbf{0}$ is locally uniformly asymptotically stable and the sway and heave relative velocities converge to zero, thus solving locally the aforementioned problem in the presence of constant unknown ocean currents.

Proof: Consider the closed-loop nonlinear system

$$\dot{\mathbf{z}} = \mathbf{f}_1\left(t, \mathbf{z}, \tilde{\mathbf{v}}_c\right), \tag{29}$$

where $u_{\mathbf{v}}$ and $\mathbf{u}_{\boldsymbol{\omega}}$ are replaced by (22) and (28), respectively, and $\tilde{\mathbf{v}}_c$ is here regarded as the system input. Following the same steps as in Theorem 1 it is straightforward to conclude that the system $\dot{\mathbf{z}} = \mathbf{f}_1\left(t, \mathbf{z}, \mathbf{0}\right)$ has a uniformly asymptotically stable equilibrium point at the origin $\mathbf{z} = \mathbf{0}$. The observer error was shown to be GES. Thus, if the system (29) is locally ISS (Input-to-State Stability) with $\tilde{\mathbf{v}}_c$ as input, it follows that the origin of the cascaded system (27) and (29) is locally uniformly asymptotically stable ([36], Lemma 5.6) and, following the same steps as in Theorem 1, the heave and sway velocities converge to zero. The remainder of the proof amounts to show that (29) is indeed locally ISS with $\tilde{\mathbf{v}}_c$ as input.

If, in some neighborhood of $(\mathbf{z} = \mathbf{0}, \tilde{\mathbf{v}}_c = \mathbf{0})$, $\mathbf{f}_1\left(t, \mathbf{z}, \tilde{\mathbf{v}}_c\right)$ is continuously differentiable and the Jacobian matrices $[\partial \mathbf{f}_1 / \partial \mathbf{z}]$ and $[\partial \mathbf{f}_1 / \partial \tilde{\mathbf{v}}_c]$ are bounded, uniformly in t, it follows that the system (29) is locally ISS (Lemma 5.4, [36]). This turns out to be true if both the linear and angular velocities, as well as the acceleration of the vehicle, are bounded, which can be shown in a neighborhood of $(\mathbf{z} = \mathbf{0}, \tilde{\mathbf{v}}_c = \mathbf{0})$.

It has been shown before that, when $\mathbf{z}$ converges to zero, (the proof is presented in Appendix I)

$$\lim_{\mathbf{z} \to \mathbf{0}} \boldsymbol{\omega} = \frac{\|\mathbf{v}_R + \mathbf{v}_c\|}{V_d \rho} \begin{bmatrix} 0 \\ w_r \\ -v_r \end{bmatrix}.$$

By continuity, it follows that, in a neighborhood of $\mathbf{z} = \mathbf{0}$, the angular velocity be written as

$$\boldsymbol{\omega} = \frac{\|\mathbf{v}_R + \mathbf{v}_c\|}{V_d \rho} \begin{bmatrix} 0 \\ w_r \\ -v_r \end{bmatrix} + \boldsymbol{\epsilon}, \tag{30}$$

where $\boldsymbol{\epsilon} = [\epsilon_p \, \epsilon_q \, \epsilon_r]^T$ and $\|\boldsymbol{\epsilon}\|$ is as small as required, depending of the radius of the neighborhood around $\mathbf{z} = \mathbf{0}$. Substituting (30) in the dynamics of the relative heave and sway velocities (17) yields

$$\begin{cases} \dot{v}_r = -\dfrac{Y_v + Y_{|v|v}|v_r| - \frac{m_u \|\mathbf{v}_R + \mathbf{v}_c\|}{V_d \rho} u_r}{m_v} v_r + \frac{m_w}{m_v} \epsilon_p w_r - \frac{m_u}{m_v} u_r \epsilon_r, \\ \dot{w}_r = -\dfrac{Z_w + Z_{|w|w}|w_r| - \frac{m_u \|\mathbf{v}_R + \mathbf{v}_c\|}{V_d \rho} u_r}{m_w} w_r - \frac{m_v}{m_w} \epsilon_p v_r + \frac{m_u}{m_w} u_r \epsilon_q \end{cases}. \tag{31}$$

Notice that $u_r = z_1 + V_d$, which allows to rewrite (31) as

$$\begin{cases} \dot{v}_r = -\dfrac{Y_v + Y_{|v|v}|v_r| - \frac{m_u \|\mathbf{v}_R + \mathbf{v}_c\|}{V_d \rho}(z_1 + V_d)}{m_v} v_r + \frac{m_w}{m_v} \epsilon_p w_r \\ \quad - \frac{m_u}{m_v}\left(z_1 + V_d\right) \epsilon_r, \\ \dot{w}_r = -\dfrac{Z_w + Z_{|w|w}|w_r| - \frac{m_u \|\mathbf{v}_R + \mathbf{v}_c\|}{V_d \rho}(z_1 + V_d)}{m_w} w_r - \frac{m_v}{m_w} \epsilon_p v_r \\ \quad + \frac{m_u}{m_w}\left(z_1 + V_d\right) \epsilon_q \end{cases}. \tag{32}$$

Consider now the Lyapunov-like function

$$V_l = \mathbf{z}_5^T \mathbf{M}_2^2 \mathbf{z}_5,$$

where $\mathbf{z}_5 = [v_r \, w_r]^T$ and $\mathbf{M}_2 = \mathrm{diag}\{\mathrm{m_v}, \mathrm{m_w}\}$. The time derivative of V_l is given by

$$\begin{aligned} \dot{V}_l \;=\; & -m_v \left[Y_v + Y_{|v|v}|v_r| - \frac{m_u \|\mathbf{v}_R + \mathbf{v}_c\|}{V_d \rho} (z_1 + V_d) \right] v_r^2 \\ & -m_w \left[Z_w + Z_{|w|w}|w_r| - \frac{m_u \|\mathbf{v}_R + \mathbf{v}_c\|}{V_d \rho} (z_1 + V_d) \right] w_r^2 \\ & +m_u \left(z_1 + V_d\right) \left(m_w \epsilon_q w_r - m_v \epsilon_r v_r\right). \end{aligned} \tag{33}$$

Recall that, since it was assumed that $V_d > V_c$, it follows that

$$\|\mathbf{v}_R + \mathbf{v}_c\| < 2V_d.$$

Thus, it is possible to write, from (33),

$$\begin{aligned} \dot{V}_l \;\leq\; & -m_v \left[Y_v + Y_{|v|v}|v_r| - \frac{2 m_u V_d}{\rho} - \frac{2 m_u}{\rho} |z_1| \right] v_r^2 \\ & -m_w \left[Z_w + Z_{|w|w}|w_r| - \frac{2 m_u V_d}{\rho} - \frac{2 m_u}{\rho} |z_1| \right] w_r^2 \\ & +m_u \left(z_1 + V_d\right) \left(m_w \epsilon_q w_r - m_v \epsilon_r v_r\right). \end{aligned} \tag{34}$$

Using Assumption (24), it is straightforward to conclude that, in some neighborhood of $\mathbf{z} = \mathbf{0}$, V_l satisfies

$$\dot{V}_l \leq -\gamma_1 V_l + \gamma_2 \sqrt{V_l},$$

for some $\gamma_1 > 0$, $\gamma_2 > 0$, which, attending to the positiveness of V_l, suffices to establish its boundedness for all time, which in turns implies that both the relative sway and heave velocities are bounded for all time in some neighborhood of $\mathbf{z} = \mathbf{0}$. On the other hand, from (30) and the boundedness of v_r and w_r, it is also immediate to conclude that the angular velocity stays bounded in a neighborhood of $\mathbf{z} = \mathbf{0}$. Finally, as $u_r = z_1 + V_r$, the relative surge velocity is also bounded, which concludes the proof since, for bounded velocities, it follows, from the dynamics of the vehicle, that the acceleration is also bounded. ■

Remark 3: The implementation of the control law requires, in addition to the USBL measurements, the attitude of the vehicle, its linear and angular velocities, and the linear accelerations, all expressed in body-fixed coordinates. The attitude and the angular velocity are available from any common Attitude and Heading Reference System (AHRS), e.g., the Seatex MRU6. The linear velocity may be obtained employing a myriad of sensors. As an example a Doppler velocity log, e.g., the Teledyne RDI Explorer DVL, may be used to measure the velocity of the vehicle, both relative and inertial. Finally, the linear acceleration is usually available from a triad of accelerometers, which is also a standard component in any inertial measurement unit (IMU), e.g. the Honeywell HG1700.IMU. An interesting and more detailed discussion on underwater sensing devices, as well as navigation techniques, can be found in [37].

Remark 4: It has been assumed throughout the paper that the mass, inertia, and damping matrices are diagonal. The derivation of the control laws is, nevertheless, general and it can be applied to any positive definite mass, inertial, or damping matrices. For non-diagonal mass matrices, the proofs regarding the stability of the various systems only change in what concerns the convergence of the heave and sway velocities if the mass matrix is not diagonal and new assumptions on the minimum radius R_{min} are required to guarantee that these variables also converge to zero. As an example, for a positive definite mass matrix

$$\mathbf{M} = \begin{bmatrix} m_{11} & m_{12} & m_{13} \\ m_{12} & m_{22} & m_{23} \\ m_{13} & m_{23} & m_{33} \end{bmatrix}$$

the convergence in the absence of ocean currents can be established for a minimum radius that, in addition to the previous condition (14), also satisfies (the proof is presented in Appendix J)

$$R_{min} > \max\left(\frac{\max(2m_{12}, m_{12}+m_{13})}{Y_{|v|v}}, \frac{\max(m_{12}+m_{13}, 2m_{13})}{Z_{|w|w}}\right).$$

VI. Simulation Results

To illustrate the performance of the proposed integrated guidance and control laws three computer simulations are presented in this section. In the simulations a simplified model of the SIRENE vehicle was used, assuming the vehicle is directly actuated in force and torque [3].

In the first simulation there are no ocean currents nor sensors noise. The vehicle starts at position $[0,\ 0,\ 50]^T$ m and the acoustic transponder is located at position $[500,\ 500,\ 500]^T$ m. The control parameters were chosen as follows: $k_1 = 0.025$, $\mathbf{K}_2 = 0.0005\mathrm{diag}(1,1,1)$, and $\mathbf{K}_3 = \mathrm{diag}(10,3,15)$. The desired velocity was set to $V_d = 2$ m/s, and a semi-spherical symmetric USBL sensor with seventeen receivers is assumed to be placed on the vehicle's nose. Fig. 4 shows the trajectory described by the vehicle, whereas Fig. 5 displays the evolution of the vehicle velocities and control inputs. From the figures

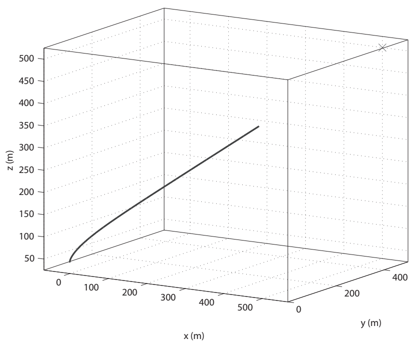

Fig. 4. Trajectory described by the vehicle in the absence of currents and noise

it can be concluded that the vehicle is driven towards the target describing a smooth trajectory. The control inputs are smooth and the resulting angular and lateral velocities converge to zero, as expected.

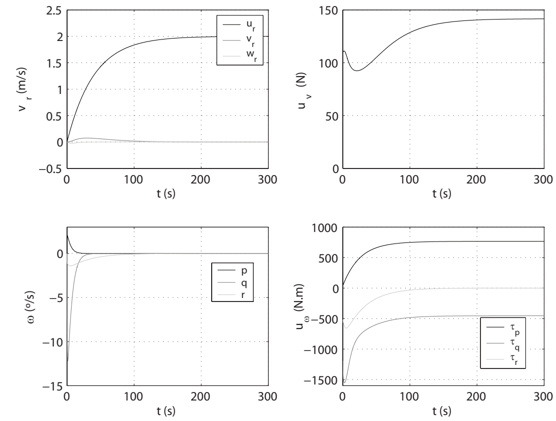

Fig. 5. Time evolution of the vehicle velocities and control inputs in the absence of ocean currents and noise

In the second simulation the vehicle has to counteract a constant unknown ocean current with velocity $[0,\ -1,\ 0]^T$m/s, expressed in the inertial frame. An observer with gain $k_{obs} = 10$ estimates this current to feed the control law, as described in Section V. The control parameters are the same as in the previous simulation. Figure 6 shows the trajectory described by the vehicle, whereas Fig. 7 displays the evolution of the vehicle velocities and control inputs. The evolution of the observer error $\tilde{\mathbf{v}}_c$ is shown in Figure 8. As expected, the

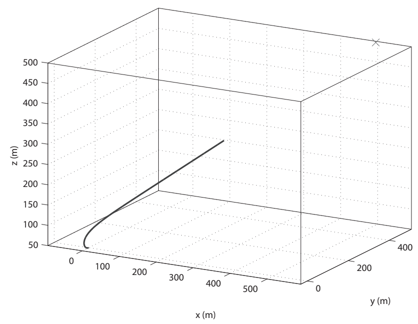

Fig. 6. Trajectory described by the vehicle in the presence of ocean currents

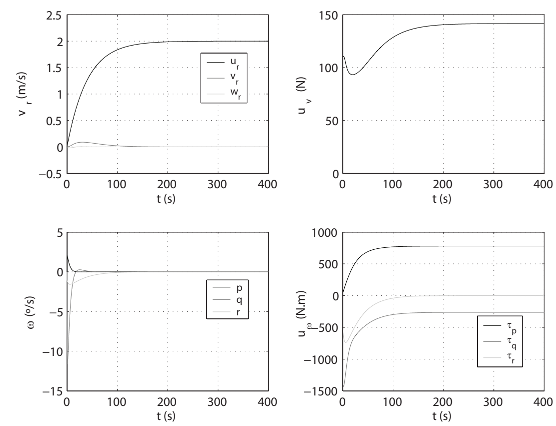

Fig. 7. Time evolution of the vehicle velocities and control inputs in the presence of ocean currents

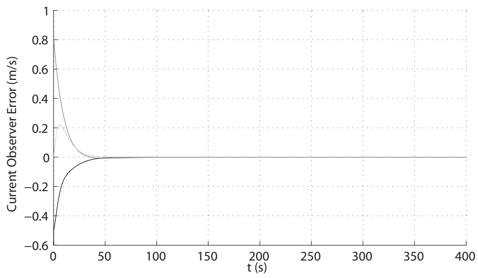

Fig. 8. Time evolution of the observer error $\tilde{\mathbf{v}_c}$.

trajectory and control inputs are smooth and the angular, sway, and heave velocities converge to zero. The observer error converges exponentially fast to zero.

The third simulation is similar to the second but sensor noise was considered, as well as saturation of the actuators. Moreover, $\pm 20\%$ parameter uncertainty was considered in the dynamics of the vehicle. The measurements of the vehicle velocity relative to the water were assumed to be corrupted by Gaussian zero-mean white noise with standard deviations of 0.01 m/s. The AHRS was assumed to provide the roll, pitch, and yaw Euler angles, also corrupted by Gaussian noises with standard deviation of $0.03\,^\circ$ for the roll and pitch and $0.3\,^\circ$ for the yaw, and the angular velocity corrupted with Gaussian noise with standard deviation of 0.1 °/s. The noise of the USBL sensor was decomposed into two components, a common mode that affects the range measurements and a differential mode, which affects the TDOA vector. For the common mode a standard deviation of 1 ms was chosen whereas for the differential mode a standard deviation of $1\mu s$ was selected. Figure 9 shows the trajectory described by the vehicle, whereas Fig. 10 displays the evolution of the vehicle velocities and control inputs. The effect of the measurement noise is visible

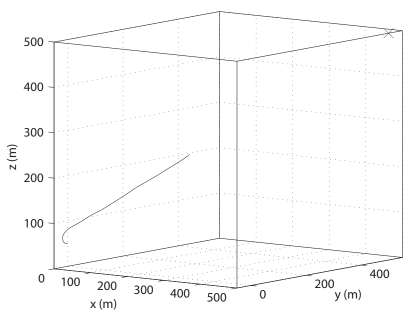

Fig. 9. Trajectory described by the vehicle in the presence of ocean currents and sensors' noise

in the evolution of the control signals but it should be noted that the trajectory described by the vehicle is not significantly affected, in spite of the presence of realistic measurement noise. The saturation effect is also noticeable during the first few seconds of the simulation, when the torque τ_q saturates. However, the attitude quickly converges to the desired one and the control enters the linear zone. It should be noticed that, if the thrust force τ_u is not enough to achieve the desired steady-state velocity V_d, the proposed solution may fail to achieve its purpose in the presence of strong ocean currents.

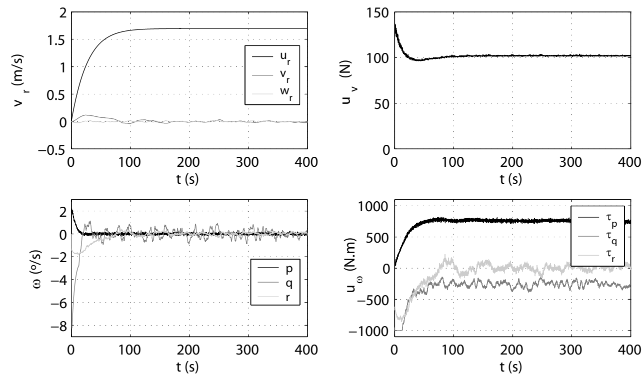

Fig. 10. Time evolution of the vehicle velocities and control inputs in the presence of ocean currents and sensors' noise

While the configuration of the USBL sensor does not affect the results of the first two simulations since these are carried out in the absence of measurement noise, it does impact the results of the third simulation since the measurements of the USBL are corrupted with noise. The semi-spherical configuration that was chosen does not favor any particular direction of the target. In the absence of strong currents the attitude of the vehicle quickly converges to a situation where the target is in a direction closer to the direction of the x axis of the vehicle. A sharp-pointed configuration of the hydrophones of the USBL would reduce the effect of the measurement noise on the overall close-loop system since this configuration privileges the directions close to the x axis of the vehicle. It would, however, increase the sensibility of the system if the initial attitude of the vehicle was such that the target was in a direction far away from the x axis of the vehicle.

VII. Conclusions

This paper presented new homing sensor based integrated guidance and control laws to drive an underactuated AUV to a fixed target in 3D using the information provided by an USBL positioning system. Under the presence (and absence) of constant known ocean currents global asymptotic stability was achieved with the proposed laws. To estimate unknown constant ocean currents a globally exponentially stable observer that also resorts to the USBL data was presented and local asymptotic stability for the overall closed-loop system was achieved. Simulation results were presented illustrating the performance of the proposed solutions under the presence of realistic sensor noise and parameter uncertainty.

References

[1] P. Sarradin, K. Leroy, H. Ondréas, M. Sibuet, M. Klages, Y. Fouquet, B. Savoye, J.-F. Drogou, and J.-L. Michel, "Evaluation of the first year of scientific use of the French ROV Victor 6000," in *Proc. 2002 International Symposium on Underwater Technology*, Tokyo, Japan, Apr. 2002, pp. 11–16.

[2] C. Silvestre and A. Pascoal, "Control of the INFANTE AUV using gain scheduled static output feedback," *Control Engineering Practice*, vol. 12, pp. 1501–1509, Dec. 2004.

[3] C. Silvestre, A. Aguiar, P. Oliveira, and A. Pascoal, "Control of the SIRENE Underwater Shuttle: System Design and Tests at Sea," in *Proc. 17th International Conference on Offshore Mechanics and Artic Engineering (OMAE 98)*, Lisbon, Portugal, Jul. 1998.

[4] A. Isidori, *Nonlinear Control Systems*, 3rd ed. Springer-Verlag, 1995.
[5] H. Nijmeijer and A. van der Schaft, *Nonlinear Dynamical Control Systems*. Springer-Verlag, 1990.
[6] S. Sastry, *Nonlinear Systems: Analysis, Stability and Control*. Springer-Verlag, 1999.
[7] K. Wichlund, O. Sørdalen, and O. Egeland, "Control of Vehicles with Second-Order Nonholonomic Constraints: Underactuated Vehicles," in *Proc. 3rd European Control Conference*, Rome, Italy, Sep. 1995, pp. 3086–3091.
[8] M. Reyhanoglu, "Control and Stabilization of an Underactuated Surface Vessel," in *Proc. 35th IEEE Conference on Decision and Control*, vol. 3, Kobe, Japan, Dec. 1996, pp. 2371–2376.
[9] K. Pettersen and H. Nijmeijer, "Global Practical Stabilization and Tracking for an Underactuated Ship - a Combined Averaging and Backstepping Approach," in *Proc. IFAC Conference on System Structure and Control*, vol. 1, Nantes, France, Jul. 1998, pp. 59–64.
[10] F. Mazenc, K. Pettersen, and H. Nijmeijer, "Global Uniform Asymptotic Stabilization of an Underactuated Surface Vessel," in *Proc. 41st IEEE Conference on Decision and Control*, vol. 1, Las Vegas, Nevada, USA, Dec. 2002, pp. 510–515.
[11] G. Indiveri, M. Aicardi, and G. Casalino, "Nonlinear Time-Invariant Feedback Control of an Underactuated Marine Vehicle Along a Straight Course," in *Proc. 5th IFAC Conference on Manoeuvring and Control of Marine Craft,*, Aalborg, Denmark, Aug. 2000, pp. 221–226.
[12] A. Aguiar and A. Pascoal, "Dynamic positioning and way-point tracking of underactuated AUVs in the presence of ocean currents," in *Proc. 41st IEEE Conference on Decision and Control*, vol. 2, Las Vegas, Nevada, USA, Dec. 2002, pp. 2105 – 2110.
[13] O.-E. Fjellstad and T. Fossen, "Position and Attitude Tracking of AUV's: A Quaternion Feedback Approach," *IEEE Journal of Oceanic Engineering*, vol. 19, no. 4, pp. 512–518, Oct. 1994.
[14] F. Alonge, F. D'Ippolito, and F. Raimondi, "Trajectory Tracking of Underactuated Underwater Vehicles," in *Proc. 40th IEEE Conference on Decision and Control*, vol. 5, Orlando, FL, USA, Jul. 2001, pp. 4421–4426.
[15] A. Aguiar and J. Hespanha, "Position Tracking of Underactuated Vehicles," in *Proc. 2003 American Control Conference*, vol. 3, Denver, Colorado, USA, Jun. 2003, pp. 1988 – 1993.
[16] M. Breivik and T. Fossen, "Guidance-Based Path Following for Autonomous Underwater Vehicles," in *Proc. MTS/IEEE OCEANS 05*, vol. 3, no. 4, Washington, D.C., USA, Sep. 2005, pp. 2807–2814.
[17] L. Lapierre, D. Soetanto, and A. Pascoal, "Nonlinear Path Following with Applications to the Control of Autonomous Underwater Vehicles," in *Proc. 42nd IEEE Conference on Decision and Control*, vol. 2, Maui, Hawaii, USA, Dec. 2003, pp. 1256–1261.
[18] N. Cowan, J. Weingarten, and D. Koditschek, "Visual Servoing via Navigation Functions," *IEEE Transactions on Robotics and Automation*, vol. 18, no. 4, pp. 521–533, Aug. 2002.
[19] E. Malis and F. Chaumette, "Theoretical improvements in the stability analysis of a new class of model-free visual servoing methods," *IEEE Transactions on Robotics and Automation*, vol. 18, no. 2, pp. 176–186, Apr. 2002.
[20] S. Cowen, S. Briest, and J. Dombrowski, "Underwater docking of autonomous undersea vehicles using optical terminal guidance," in *Proc. MTS/IEEE OCEANS 97*, vol. 2, Halifax, Canada, Oct. 1997, pp. 1143–1147.
[21] M. Feezor, F. Sorrell, P. Blankinship, and J. Bellingham, "Autonomous underwater vehicle homing/docking via electromagnetic guidance," *IEEE Journal of Oceanic Engineering*, vol. 26, no. 4, pp. 515–521, Oct. 2001.
[22] P. Jantapremjit and P. Wilson, "Control and Guidance for Homing and Docking Tasks using an Autonomous Underwater Vehicle," in *Proc. IEEE/RSJ Int. Conf. Intelligent Robots and Systems*, San Diego, CA, USA, Oct. 2007, pp. 3672–3677.
[23] J.-Y. Park, H.-H. Jun, P.-M. Lee, F.-Y. Lee, and J.-H. Oh, "Experiment on Underwater Docking of an Autonomous Underwater Vehicle 'ISiMI' using Optical Terminal Guidance," in *Proc. OCEANS 2007*, vol. 2, Vancouver, BC, Canada, Jun. 2007, pp. 1–6.
[24] J. Vaganay, P. Baccou, and B. Jouvencel, "Homing by Acoustic Ranging to a Single Beacon," in *Proc. OCEANS 2000 MTS/IEEE Conference and Exhibition*, vol. 2, Vancouver, BC, Canada, Sep. 2000, pp. 1457–1462.
[25] P. Baccou and B. Jouvencel, "Homing and navigation using one transponder for AUV, postprocessing comparisons results with long base-line navigation," in *Proc. ICRA '02 - IEEE Int. Conf. Robotics and Automation, 2002*, vol. 4, Washington D.C., USA, May 2002, pp. 4004–4009.
[26] C. Mayhew, R. Sanfelice, and A. Teel, "Robust Source-Seeking Hybrid Controllers for Autonomous Vehicles," in *Proc. American Control Conference, 2007 - ACC '07*, New York City, USA, Jul. 2007, pp. 1185–1190.
[27] A. Gadre and D. Stilwell, "Underwater Navigation In the Presence of Unknown Currents Based on Range Measurements From a Single Location," in *Proc. American Control Conference, 2005*, vol. 1, Portland, OR, USA, Jun. 2005, pp. 656–661.
[28] J. Refsnes, K. Pettersen, and A. Sørensen, "Observer Design for Underwater Vehicles with Position and Angle Measurement," in *Proc. 7th Conf. on Manoeuvring and Control of Marine Craft (MCMC2006)*, Lisbon, Portugal, Sep. 2006.
[29] P. Batista, C. Silvestre, and P. Oliveira, "A Sensor Based Homing Strategy for Autonomous Underwater Vehicles," in *Proc. MED2006 - 14th Mediterranean Conference on Control and Automation*, Ancona, Italy, Jun. 2006.
[30] ——, "A Quaternion Sensor Based Controller for Homing of Underactuated AUVs," in *Proc. 45th IEEE Conference on Decision and Control*, San Diego, USA, Dec. 2006, pp. 51–56.
[31] P. Rigby, O. Pizarro, and S. Williams, "Towards Geo-Referenced AUV Navigation Through Fusion of USBL and DVL Measurements," in *Proc. MTS/IEEE OCEANS 2006*, Boston, USA, Sep. 2006.
[32] T. Fossen, *Guidance and Control of Ocean Vehicles*. Wiley, 1994.
[33] J. Buchanan, R. Gilbert, A. Wirgin, and Y. Xu, *Marine Acoustics, Direct and Inverse Problems*. SIAM, Philadelphia, 2004.
[34] A. Isidori, L. Marconi, and A. Serrani, *Robust Autonomous Guidance*. Springer-Verlag, 2003.
[35] M. Kritić, I. Kanellakopoulos, and P. Kokotović, *Nonlinear and Adaptive Control Design*. Wiley-Intersciencec, 1995.
[36] H. Khalil, *Nonlinear Systems*, 2nd ed. Prentice-Hall, 1996.
[37] J. Kinsey, R. Eustice, and L. Whitcomb, "A Survey of Underwater Vehicle Navigation: Recent Advances and New Challenges," in *Proc. 7th IFAC Conference on Manoeuvring and Control of Marine Craft (MCMC2006)*, Lisboa, Portugal, Sep. 2006.

Appendix A
Time derivative of $\mathbf{d}$

Denote by $\mathbf{e}$ the position of the target expressed in body-fixed coordinates. As the target is assumed to be fixed in the world, the time derivative of $\mathbf{e}$ is simply given by

$$\dot{\mathbf{e}} = -\mathbf{v} - \mathbf{S}(\boldsymbol{\omega})\,\mathbf{e}. \tag{35}$$

The direction of the target $\mathbf{d}$ can be directly expressed in terms of the position of the emitter,

$$\mathbf{d} = \frac{1}{\|\mathbf{e}\|}\mathbf{e}. \tag{36}$$

Taking the time derivative of (36) yields

$$\dot{\mathbf{d}} = \frac{\dot{\mathbf{e}}\,\|\mathbf{e}\| - \dot{\|\mathbf{e}\|}\mathbf{e}}{\|\mathbf{e}\|^2} = \frac{1}{\rho}\dot{\mathbf{e}} - \frac{\dot{\rho}}{\rho^2}\mathbf{e}, \tag{37}$$

where the distance to the target $\|\mathbf{e}\|$ was replaced by ρ. Substituting (35) and (36) in (37) gives

$$\dot{\mathbf{d}} = \frac{1}{\rho}\left[-\mathbf{v} - \mathbf{S}(\boldsymbol{\omega})\,\mathbf{e}\right] - \frac{\dot{\rho}}{\rho}\mathbf{d} = \frac{1}{\rho}\left[-\mathbf{v} - \dot{\rho}\mathbf{d}\right] - \mathbf{S}(\boldsymbol{\omega})\,\mathbf{d}. \tag{38}$$

The derivative of ρ can be easily computed observing that $\rho = \sqrt{\mathbf{e}^T\mathbf{e}}$, which gives

$$\dot{\rho} = -\mathbf{d}^T\mathbf{v}. \tag{39}$$

Substituting (39) in (38) gives

$$\dot{\mathbf{d}} = \frac{1}{\rho}\left[-\mathbf{v} + \left(\mathbf{d}^T\mathbf{v}\right)\mathbf{d}\right] - \mathbf{S}(\boldsymbol{\omega})\,\mathbf{d}. \tag{40}$$

Finally, using Lagrange's formula, (40) can be rewritten as

$$\dot{\mathbf{d}} = \frac{1}{\rho}\mathbf{S}(\mathbf{v}\times\mathbf{d})\,\mathbf{d} - \mathbf{S}(\boldsymbol{\omega})\,\mathbf{d} = \mathbf{S}(\boldsymbol{\omega}_g)\,\mathbf{d},$$

where

$$\boldsymbol{\omega}_g := -\boldsymbol{\omega} + \frac{1}{\rho}\mathbf{v} \times \mathbf{d}.$$

APPENDIX B
TIME DERIVATIVE OF $\mathbf{q}$

The quaternion q is such that it represents the rotation $\mathbf{R}_e$ that satisfies (6),

$$\mathbf{R}_e[1,0,0]^T := -\mathbf{H}_Q^{-1}\mathbf{H}_R^T\boldsymbol{\Delta}, \tag{41}$$

and is smooth over time, which is possible as the right side of (41) is continuous and continuously differentiable. Notice that the right side of (41) corresponds to the direction of the target $\mathbf{d}$ and its time derivative is given by (5).

Taking the time derivative of both sides of (41) yields

$$\dot{\mathbf{R}}_e[1,0,0]^T = \dot{\mathbf{d}}. \tag{42}$$

Substituting (5) in (42) gives

$$\dot{\mathbf{R}}_e[1,0,0]^T = \mathbf{S}\left(\boldsymbol{\omega}_g\right)\mathbf{d}. \tag{43}$$

Recalling that the right side of (41) corresponds to the direction of the target, it is possible to rewrite (43) as

$$\dot{\mathbf{R}}_e[1,0,0]^T = \mathbf{S}\left(\boldsymbol{\omega}_g\right)\mathbf{R}_e[1,0,0]^T. \tag{44}$$

From the comparison of both sides of (44) it is straightforward to conclude that the time derivative of $\mathbf{R}_e$ is given by

$$\dot{\mathbf{R}}_e = \mathbf{S}\left(\boldsymbol{\omega}_g\right)\mathbf{R}_e. \tag{45}$$

The time derivative of the quaternion that represents a rotation matrix with dynamics (45) is given by

$$\dot{\mathbf{q}} = \frac{1}{2}\mathbf{D}(\boldsymbol{\omega}_g)\mathbf{q},$$

where

$$\mathbf{D}(\boldsymbol{\omega}_g) = \begin{bmatrix} 0 & -\boldsymbol{\omega}_g^T \\ \boldsymbol{\omega}_g & \mathbf{S}(\boldsymbol{\omega}_g) \end{bmatrix}.$$

APPENDIX C
TIME DERIVATIVE OF V_1

Taking the time derivative of V_1 gives

$$\dot{V}_1 = z_1\dot{z}_1 + 2z_2\dot{z}_2 + 2\mathbf{z}_3^T\dot{\mathbf{z}}_3 = z_1[1,\,0,\,0]\dot{\mathbf{v}} + 2z_2\dot{q}_0 + 2\mathbf{z}_3^T\dot{\mathbf{q}}_v. \tag{46}$$

Substituting the dynamics of $\mathbf{v}$, (2), and the quaternion dynamics, (10), in (46), and simplifying, yields

$$\begin{aligned}\dot{V}_1 \;=\;& z_1[1,\,0,\,0]\mathbf{M}^{-1}\left[-\mathbf{S}(\boldsymbol{\omega})\mathbf{M}\mathbf{v} - \mathbf{D}_{\mathbf{v}}(\mathbf{v})\mathbf{v} + \mathbf{b}_{\mathbf{v}}u_{\mathbf{v}}\right] \\ &+2z_2\left(-\frac{1}{2}\boldsymbol{\omega}_g^T\mathbf{q}_v\right) + 2\mathbf{z}_3^T\left(\frac{1}{2}\boldsymbol{\omega}_g q_0 + \frac{1}{2}\mathbf{S}\left(\boldsymbol{\omega}_g\right)\mathbf{q}_v\right) \\ =\;& z_1[1,\,0,\,0]\mathbf{M}^{-1}\mathbf{b}_{\mathbf{v}}u_{\mathbf{v}} \\ &-z_1[1,\,0,\,0]\mathbf{M}^{-1}\left[\mathbf{S}(\boldsymbol{\omega})\mathbf{M}\mathbf{v} + \mathbf{D}_{\mathbf{v}}(\mathbf{v})\mathbf{v}\right] \\ &-z_2\boldsymbol{\omega}_g^T\mathbf{q}_v + q_0\mathbf{z}_3^T\boldsymbol{\omega}_g + \mathbf{z}_3^T\mathbf{S}\left(\boldsymbol{\omega}_g\right)\mathbf{q}_v.\end{aligned} \tag{47}$$

Since $\mathbf{z}_3 = \mathbf{q}_v$ and $\mathbf{x}^T\mathbf{S}\left(\mathbf{y}\right)\mathbf{x} = 0, \ \forall\mathbf{x},\mathbf{y} \in \mathbb{R}^3$, (47) simplifies to

$$\begin{aligned}\dot{V}_1 \;=\;& z_1[1,\,0,\,0]\mathbf{M}^{-1}\mathbf{b}_{\mathbf{v}}u_{\mathbf{v}} \\ &-z_1[1,\,0,\,0]\mathbf{M}^{-1}\left[\mathbf{S}(\boldsymbol{\omega})\mathbf{M}\mathbf{v} + \mathbf{D}_{\mathbf{v}}(\mathbf{v})\mathbf{v}\right] \\ &-z_2\boldsymbol{\omega}_g^T\mathbf{z}_3 + q_0\mathbf{z}_3^T\boldsymbol{\omega}_g.\end{aligned} \tag{48}$$

Now, substituting $z_2 = q_0 - 1$ and $\boldsymbol{\omega}_g = -\boldsymbol{\omega} + \boldsymbol{\omega}_l$ in (48) finally yields

$$\begin{aligned}\dot{V}_1 \;=\;& z_1[1,\,0,\,0]\mathbf{M}^{-1}\mathbf{b}_{\mathbf{v}}u_{\mathbf{v}} \\ &-z_1[1,\,0,\,0]\mathbf{M}^{-1}\left[\mathbf{S}(\boldsymbol{\omega})\mathbf{M}\mathbf{v} + \mathbf{D}_{\mathbf{v}}(\mathbf{v})\mathbf{v}\right] \\ &+\mathbf{z}_3^T\left(-\boldsymbol{\omega} + \boldsymbol{\omega}_l\right).\end{aligned} \tag{49}$$

APPENDIX D
TIME DERIVATIVE OF V_2

Taking the time derivative of V_2 gives

$$\dot{V}_2 = \dot{V}_1 + \mathbf{z}_4^T\left(\dot{\boldsymbol{\omega}} - \dot{\boldsymbol{\omega}}_d\right). \tag{50}$$

Substituting (2) and (49) in (50) yields

$$\begin{aligned}\dot{V}_2 \;=\;& z_1[1,\,0,\,0]\mathbf{M}^{-1}\mathbf{b}_{\mathbf{v}}u_{\mathbf{v}} \\ &-z_1[1,\,0,\,0]\mathbf{M}^{-1}\left[\mathbf{S}(\boldsymbol{\omega})\mathbf{M}\mathbf{v} + \mathbf{D}_{\mathbf{v}}(\mathbf{v})\mathbf{v} + \mathbf{g}_{\mathbf{v}}(\mathbf{R})\right] \\ &+\mathbf{z}_3^T\left(-\boldsymbol{\omega} + \boldsymbol{\omega}_l\right) \\ &+\mathbf{z}_4^T\left(\mathbf{J}^{-1}\left[-\mathbf{S}(\mathbf{v})\mathbf{M}\mathbf{v} - \mathbf{S}(\boldsymbol{\omega})\mathbf{J}\boldsymbol{\omega} - \mathbf{D}_{\boldsymbol{\omega}}(\boldsymbol{\omega})\boldsymbol{\omega}\right.\right. \\ &\left.\left.-\mathbf{g}_{\boldsymbol{\omega}}(\mathbf{R}) + \mathbf{u}_{\boldsymbol{\omega}}\right] - \dot{\boldsymbol{\omega}}_d\right).\end{aligned} \tag{51}$$

Now, substituting (11) and using $\mathbf{z}_4 = \boldsymbol{\omega} - \boldsymbol{\omega}_d$ in (51) finally gives

$$\begin{aligned}\dot{V}_2 \;=\;& -k_1z_1^2 - \mathbf{z}_3^T\mathbf{K}_2\mathbf{z}_3 \\ &+\mathbf{z}_4^T\left(\mathbf{J}^{-1}\left[-\mathbf{S}(\mathbf{v})\mathbf{M}\mathbf{v} - \mathbf{S}(\boldsymbol{\omega})\mathbf{J}\boldsymbol{\omega} - \mathbf{D}_{\boldsymbol{\omega}}(\boldsymbol{\omega})\boldsymbol{\omega}\right.\right. \\ &\left.\left.-\mathbf{g}_{\boldsymbol{\omega}}(\mathbf{R}) + \mathbf{u}_{\boldsymbol{\omega}}\right] - \dot{\boldsymbol{\omega}}_d - \mathbf{z}_3\right).\end{aligned}$$

APPENDIX E
CLOSED-LOOP ERROR DYNAMICS

This section presents the derivation of the closed-loop error dynamics in the absence of ocean currents, as derived in Section IV. The equations are identical in the presence of known ocean currents since only the definition of the attitude and surge velocity error variables change.

The time derivative of z_1 is given by

$$\dot{z}_1 = [1,\,0,\,0]\dot{\mathbf{v}}. \tag{52}$$

Substituting (2) in (52) gives

$$\dot{z}_1 = [1,\,0,\,0]\mathbf{M}^{-1}\left[-\mathbf{S}(\boldsymbol{\omega})\mathbf{M}\mathbf{v} - \mathbf{D}_{\mathbf{v}}(\mathbf{v})\mathbf{v} + \mathbf{b}_{\mathbf{v}}u_{\mathbf{v}}\right]. \tag{53}$$

With the control law (11) it follows, from (53), that

$$\dot{z}_1 = -k_1z_1.$$

From (8) and (10) the time derivative of z_2 can be written as

$$\dot{z}_2 = -\frac{1}{2}\boldsymbol{\omega}_g^T\mathbf{q}_v. \tag{54}$$

Now, notice that $\mathbf{z}_3 = \mathbf{q}_v$. Thus, (54) can be rewritten as

$$\dot{z}_2 = -\frac{1}{2}\boldsymbol{\omega}_g^T\mathbf{z}_3. \tag{55}$$

On the other hand, from the definitions of $\boldsymbol{\omega}_g$, $\mathbf{z}_4$, and $\boldsymbol{\omega}_d$, it follows that

$$\boldsymbol{\omega}_g = -\left(\mathbf{K}_2\mathbf{z}_3 + \mathbf{z}_4\right) \tag{56}$$

Substituting (56) in (55) gives

$$\dot{z}_2 = \frac{1}{2}\left(\mathbf{K}_2\mathbf{z}_3 + \mathbf{z}_4\right)^T\mathbf{z}_3.$$

Since $\mathbf{K}_2$ is symmetric, it is finally possible to write

$$\dot{z}_2 = \frac{1}{2}\left(\mathbf{z}_3^T \mathbf{K}_2 \mathbf{z}_3 + \mathbf{z}_3^T \mathbf{z}_4\right).$$

From (9) and (10) the dynamics of $\mathbf{z}_3$ are simply given by

$$\dot{\mathbf{z}}_3 = \frac{1}{2}\left[q_0 \boldsymbol{\omega}_g + \mathbf{S}(\boldsymbol{\omega}_g)\mathbf{z}_3\right]. \tag{57}$$

Substituting (56) in (57) yields

$$\dot{\mathbf{z}}_3 = -\frac{1}{2}\left[q_0(\mathbf{K}_2\mathbf{z}_3 + \mathbf{z}_4) + \mathbf{S}(\mathbf{K}_2\mathbf{z}_3 + \mathbf{z}_4)\mathbf{z}_3\right]. \tag{58}$$

From the definition of z_2 it follows that $q_o = z_2 + 1$. Thus, is finally possible to write (58) as

$$\dot{\mathbf{z}}_3 = -\frac{1}{2}\left[(z_2+1)(\mathbf{K}_2\mathbf{z}_3 + \mathbf{z}_4) + \mathbf{S}(\mathbf{K}_2\mathbf{z}_3 + \mathbf{z}_4)\mathbf{z}_3\right].$$

The time derivative of $\mathbf{z}_4$ is given, from (12), by

$$\dot{\mathbf{z}}_4 = \dot{\boldsymbol{\omega}} - \dot{\boldsymbol{\omega}}_d. \tag{59}$$

Substituting (2) in (59) gives

$$\dot{\mathbf{z}}_4 = -\mathbf{S}(\mathbf{v})\mathbf{M}\mathbf{v} - \mathbf{S}(\boldsymbol{\omega})\mathbf{J}\boldsymbol{\omega} - \mathbf{D}_{\boldsymbol{\omega}}(\boldsymbol{\omega})\boldsymbol{\omega} - \mathbf{g}_{\boldsymbol{\omega}}(\mathbf{R}) + \mathbf{u}_{\boldsymbol{\omega}} - \dot{\boldsymbol{\omega}}_d. \tag{60}$$

With the control law (13), the dynamics of $\mathbf{z}_4$ become

$$\dot{\mathbf{z}}_4 = \mathbf{z}_3 - \mathbf{K}_3\mathbf{z}_4.$$

Appendix F
Limit of $\boldsymbol{\omega}$ when $\mathbf{z} \to \mathbf{0}$

When $\mathbf{z}$ converges to zero, so does $\mathbf{z}_4$, from which it is straightforward to conclude that $\boldsymbol{\omega} \to \boldsymbol{\omega}_d$. Since

$$\boldsymbol{\omega}_d = \mathbf{K}_2\mathbf{z}_3 + \boldsymbol{\omega}_l = \mathbf{K}_2\mathbf{z}_3 + \mathbf{v} \times \mathbf{d}/\rho$$

and $\mathbf{z}_3 \to \mathbf{0}$, it follows that $\boldsymbol{\omega} \to \boldsymbol{\omega}_l$. Now, as it was seen, when $\mathbf{z} \to \mathbf{0}$, it is true that $\mathbf{R}_e \to \mathbf{I}$ from which it can be concluded that $\mathbf{d} \to [1,0,0]^T$. Thus,

$$\lim_{\mathbf{z}\to\mathbf{0}} \boldsymbol{\omega} = \frac{1}{\rho}\mathbf{v} \times [1,0,0]^T = \frac{1}{\rho}[0, w, -v]^T.$$

Appendix G
Positiveness of the first component of ${}^E\!\left(\mathbf{v}_r^O\right)$

To show that the first component of ${}^E\!\left(\mathbf{v}_r^O\right)$ is always positive under the assumption

$$V_d > V_c, \tag{61}$$

compute the inner product between ${}^E\!\left(\mathbf{v}_r^O\right)$ and $[1,0,0]^T$,

$${}^E\!\left(\mathbf{v}_r^O\right) \cdot [1,0,0]^T = {}^E\!\left(\mathbf{v}_r^O\right)^T [1,0,0]^T. \tag{62}$$

Taking into account (19) and (20) it is possible to rewrite (62) as

$$\begin{aligned}
{}^E\!\left(\mathbf{v}_r^O\right) \cdot [1,0,0]^T &= {}^E\!\left(\mathbf{v}_r^O\right)^T {}^E(\mathbf{d}) \\
&= {}^E\!\left(\mathbf{v}_r^O\right)^T \frac{{}^E(\mathbf{v}_r^O) + {}^E(\mathbf{v}_c)}{\| {}^E(\mathbf{v}_r^O) + {}^E(\mathbf{v}_c)\|}.
\end{aligned} \tag{63}$$

Now, as $\left\|\mathbf{v}_r^O\right\| = V_d$, $\|\mathbf{v}_c\| = V_c$, and using the inner product properties in (63) yields

$$\begin{aligned}
{}^E\!\left(\mathbf{v}_r^O\right) \cdot [1,0,0]^T &= \frac{V_d\left(V_d + V_c \cos\left[\angle({}^E(\mathbf{v}_r^O), \mathbf{v}_c)\right]\right)}{\| {}^E(\mathbf{v}_r^O) + {}^E(\mathbf{v}_c)\|} \\
&\geq \frac{V_d}{\| {}^E(\mathbf{v}_r^O) + {}^E(\mathbf{v}_c)\|}(V_d - V_c).
\end{aligned} \tag{64}$$

From (61) and (64) it follows that

$${}^E\!\left(\mathbf{v}_r^O\right) \cdot [1,0,0]^T > 0. \tag{65}$$

Appendix H
Induced rotation velocity $\boldsymbol{\omega}_l$ in the presence of ocean currents

In the presence of currents the rotation matrix $\mathbf{R}_e$ is implicitly defined by (21),

$$\mathbf{R}_e[V_d, 0, 0]^T = \mathbf{v}_r^O, \tag{66}$$

where $\mathbf{v}_r^O$ satisfies

$$\frac{\mathbf{v}_r^O + \mathbf{v}_c}{\|\mathbf{v}_r^O + \mathbf{v}_c\|} = \mathbf{d}. \tag{67}$$

To compute the time derivative of the right side of (66), take the time derivative of both sides of (67),

$$\frac{d}{dt}\left(\frac{\mathbf{v}_r^O + \mathbf{v}_c}{\|\mathbf{v}_r^O + \mathbf{v}_c\|}\right) = \dot{\mathbf{d}}$$

$$\Leftrightarrow \frac{(\dot{\mathbf{v}}_r^O + \dot{\mathbf{v}}_c)}{\|\mathbf{v}_r^O + \mathbf{v}_c\|} - \frac{\frac{(\mathbf{v}_r^O + \mathbf{v}_c)^T(\dot{\mathbf{v}}_r^O + \dot{\mathbf{v}}_c)}{\sqrt{(\mathbf{v}_r^O + \mathbf{v}_c)^T(\mathbf{v}_r^O + \mathbf{v}_c)}}(\mathbf{v}_r^O + \mathbf{v}_c)}{\|\mathbf{v}_r^O + \mathbf{v}_c\|^2} = \dot{\mathbf{d}}. \tag{68}$$

Using (67) it is possible to simplify (68), which gives

$$\frac{\dot{\mathbf{v}}_r^O + \dot{\mathbf{v}}_c - \mathbf{d}^T\left(\dot{\mathbf{v}}_r^O + \dot{\mathbf{v}}_c\right)\mathbf{d}}{\|\mathbf{v}_r^O + \mathbf{v}_c\|} = \dot{\mathbf{d}}. \tag{69}$$

The time derivative of the velocity of the ocean current, considering that this vector is constant in the inertial frame, is simply given by

$$\dot{\mathbf{v}}_c = -\mathbf{S}(\boldsymbol{\omega})\mathbf{v}_c. \tag{70}$$

Let

$$\dot{\mathbf{v}}_r^O = -\mathbf{S}(\boldsymbol{\omega})\mathbf{v}_r^O - \frac{\|\mathbf{v}_r^O + \mathbf{v}_c\|}{\rho}\mathbf{v} + \alpha\mathbf{d} + \beta_1\mathbf{d}^{\perp_1} + \beta_2\mathbf{d}^{\perp_2}, \tag{71}$$

where α, β_1, $\beta_2 \in \mathbb{R}$ and $\mathbf{d}$, $\mathbf{d}^{\perp_1}$, $\mathbf{d}^{\perp_2}$ form a basis for $\mathbb{R}^3$, with $\mathbf{d}^{\perp_1} \perp \mathbf{d}$, $\mathbf{d}^{\perp_2} \perp \mathbf{d}$, and $\mathbf{d}^{\perp_1} \perp \mathbf{d}^{\perp_2}$. Substituting (40), (70), and (71) in (69) yields

$$\begin{aligned}
&\frac{-\mathbf{S}(\boldsymbol{\omega})\mathbf{v}_r^O - \frac{\|\mathbf{v}_r^O + \mathbf{v}_c\|}{\rho}\mathbf{v} + \alpha\mathbf{d} + \beta_1\mathbf{d}^{\perp_1} + \beta_2\mathbf{d}^{\perp_2}}{\|\mathbf{v}_r^O + \mathbf{v}_c\|} \\
&+ \frac{-\mathbf{S}(\boldsymbol{\omega})\mathbf{v}_c + \left[\mathbf{d}^T\mathbf{S}(\boldsymbol{\omega})\mathbf{v}_r^O\right]\mathbf{d} + \frac{\|\mathbf{v}_r^O + \mathbf{v}_c\|}{\rho}\left(\mathbf{d}^T\mathbf{v}\right)\mathbf{d}}{\|\mathbf{v}_r^O + \mathbf{v}_c\|} \\
&- \frac{\alpha\left(\mathbf{d}^T\mathbf{d}\right)\mathbf{d} + \beta_1\left(\mathbf{d}^T\mathbf{d}^{\perp_1}\right)\mathbf{d} + \beta_2\left(\mathbf{d}^T\mathbf{d}^{\perp_2}\right)\mathbf{d}}{\|\mathbf{v}_r^O + \mathbf{v}_c\|} \\
&+ \frac{\left[\mathbf{d}^T\mathbf{S}(\boldsymbol{\omega})\mathbf{v}_c\right]\mathbf{d}}{\|\mathbf{v}_r^O + \mathbf{v}_c\|} = \frac{1}{\rho}\left[-\mathbf{v} + \left(\mathbf{d}^T\mathbf{v}\right)\mathbf{d}\right] - \mathbf{S}(\boldsymbol{\omega})\mathbf{d}.
\end{aligned} \tag{72}$$

Since $\mathbf{d}$ is a unit vector, $\mathbf{d} \perp \mathbf{d}^{\perp_1}$, and $\mathbf{d} \perp \mathbf{d}^{\perp_2}$, (72) simplifies to

$$\begin{aligned}
&\frac{-\mathbf{S}(\boldsymbol{\omega})\mathbf{v}_r^O - \frac{\|\mathbf{v}_r^O + \mathbf{v}_c\|}{\rho}\mathbf{v} + \beta_1\mathbf{d}^{\perp_1} + \beta_2\mathbf{d}^{\perp_2} - \mathbf{S}(\boldsymbol{\omega})\mathbf{v}_c}{\|\mathbf{v}_r^O + \mathbf{v}_c\|} \\
&+ \frac{\left[\mathbf{d}^T\mathbf{S}(\boldsymbol{\omega})\mathbf{v}_r^O\right]\mathbf{d} + \frac{\|\mathbf{v}_r^O + \mathbf{v}_c\|}{\rho}\left(\mathbf{d}^T\mathbf{v}\right)\mathbf{d}}{\|\mathbf{v}_r^O + \mathbf{v}_c\|} \\
&+ \frac{\left[\mathbf{d}^T\mathbf{S}(\boldsymbol{\omega})\mathbf{v}_c\right]\mathbf{d}}{\|\mathbf{v}_r^O + \mathbf{v}_c\|} = \frac{1}{\rho}\left[-\mathbf{v} + \left(\mathbf{d}^T\mathbf{v}\right)\mathbf{d}\right] - \mathbf{S}(\boldsymbol{\omega})\mathbf{d}.
\end{aligned} \tag{73}$$

After a few more algebraic manipulations (73) simplifies to

$$\frac{-\mathbf{S}(\boldsymbol{\omega})\mathbf{v}_r^O+\beta_1\mathbf{d}^{\perp_1}+\beta_2\mathbf{d}^{\perp_2}-\mathbf{S}(\boldsymbol{\omega})\mathbf{v}_c}{\|\mathbf{v}_r^O+\mathbf{v}_c\|} + \frac{\left[\mathbf{d}^T\mathbf{S}(\boldsymbol{\omega})\mathbf{v}_r^O\right]\mathbf{d}+\left[\mathbf{d}^T\mathbf{S}(\boldsymbol{\omega})\mathbf{v}_c\right]\mathbf{d}}{\|\mathbf{v}_r^O+\mathbf{v}_c\|} = -\mathbf{S}(\boldsymbol{\omega})\,\mathbf{d}. \tag{74}$$

Using (67) it follows from (74) that

$$\frac{\beta_1\mathbf{d}^{\perp_1}+\beta_2\mathbf{d}^{\perp_2}+\left[\mathbf{d}^T\mathbf{S}(\boldsymbol{\omega})\,\mathbf{v}_r^O\right]\mathbf{d}+\left[\mathbf{d}^T\mathbf{S}(\boldsymbol{\omega})\,\mathbf{v}_c\right]\mathbf{d}}{\|\mathbf{v}_r^O+\mathbf{v}_c\|} = \mathbf{0}. \tag{75}$$

Since $\left[\mathbf{d}^T\mathbf{S}(\boldsymbol{\omega})\,\mathbf{v}_r^O\right] = -\left[\mathbf{d}^T\mathbf{S}(\boldsymbol{\omega})\,\mathbf{v}_c\right]$, (75) simplifies to

$$\frac{\beta_1\mathbf{d}^{\perp_1}+\beta_2\mathbf{d}^{\perp_2}}{\|\mathbf{v}_r^O+\mathbf{v}_c\|} = \mathbf{0}. \tag{76}$$

Now, as $\mathbf{d}^{\perp_1}\perp\mathbf{d}^{\perp_2}$, if follows from (76) that

$$\beta_1 = \beta_2 = 0.$$

Thus, the time derivative of $\mathbf{v}_r^O$ is given by

$$\dot{\mathbf{v}}_r^O = -\mathbf{S}(\boldsymbol{\omega})\,\mathbf{v}_r^O - \frac{\|\mathbf{v}_r^O+\mathbf{v}_c\|}{\rho}\mathbf{v}+\alpha\mathbf{d} \tag{77}$$

for some $\alpha\in\mathbb{R}$.

To compute α recall that $\mathbf{v}_r^O$ is a vector with constant norm. Therefore,

$$\left(\mathbf{v}_r^O\right)^T\dot{\mathbf{v}}_r^O = 0. \tag{78}$$

Substituting (77) in (78) yields

$$\begin{aligned}
&\left(\mathbf{v}_r^O\right)^T\left[-\mathbf{S}(\boldsymbol{\omega})\,\mathbf{v}_r^O - \frac{\|\mathbf{v}_r^O+\mathbf{v}_c\|}{\rho}\mathbf{v}+\alpha\mathbf{d}\right] = 0\\
\Leftrightarrow\quad & -\left(\mathbf{v}_r^O\right)^T\mathbf{S}(\boldsymbol{\omega})\,\mathbf{v}_r^O\\
&-\frac{\|\mathbf{v}_r^O+\mathbf{v}_c\|}{\rho}\left(\mathbf{v}_r^O\right)^T\mathbf{v}+\alpha\left(\mathbf{v}_r^O\right)^T\mathbf{d} = 0.
\end{aligned} \tag{79}$$

Since $\mathbf{x}^T\mathbf{S}(\mathbf{y})\,\mathbf{x}=0,\ \forall\mathbf{x},\mathbf{y}\in\mathbb{R}^3$, it follows from (79) that

$$\alpha = \frac{\|\mathbf{v}_r^O+\mathbf{v}_c\|}{\rho}\frac{\left(\mathbf{v}_r^O\right)^T\mathbf{v}}{\left(\mathbf{v}_r^O\right)^T\mathbf{d}}. \tag{80}$$

Notice that α is well defined as $\left(\mathbf{v}_r^O\right)^T\mathbf{d}$ is strictly positive. This can be easily seen as

$$\begin{aligned}
\left(\mathbf{v}_r^O\right)^T\mathbf{d} &= \mathbf{v}_r^O\cdot\mathbf{d}\\
&= {}^E\!\left(\mathbf{v}_r^O\right)\cdot{}^E(\mathbf{d})\\
&= {}^E\!\left(\mathbf{v}_r^O\right)\cdot[1,0,0]^T,
\end{aligned}$$

which was seen to be stricty positive in Appendix G. The time derivative of $\mathbf{v}_r^O$ can then be written as

$$\dot{\mathbf{v}}_r^O = -\mathbf{S}(\boldsymbol{\omega})\,\mathbf{v}_r^O - \frac{\|\mathbf{v}_r^O+\mathbf{v}_c\|}{\rho}\left[\mathbf{v}-\frac{\left(\mathbf{v}_r^O\right)^T\mathbf{v}}{\left(\mathbf{v}_r^O\right)^T\mathbf{d}}\mathbf{d}\right]. \tag{81}$$

Finally, using Lagrange's formula, (81) can be rewritten as

$$\dot{\mathbf{v}}_r^O = \mathbf{S}\left(-\boldsymbol{\omega}-\frac{\|\mathbf{v}_r^O+\mathbf{v}_c\|}{V_d^2\rho}\mathbf{v}_r^O\times\left[\mathbf{v}-\frac{\left(\mathbf{v}_r^O\right)^T\mathbf{v}}{\left(\mathbf{v}_r^O\right)^T\mathbf{d}}\mathbf{d}\right]\right)\mathbf{v}_r^O. \tag{82}$$

Indeed, expanding (82) yields

$$\begin{aligned}
\dot{\mathbf{v}}_r^O &= -\frac{\|\mathbf{v}_r^O+\mathbf{v}_c\|}{V_d^2\rho}\left(\mathbf{v}_r^O\times\left[\mathbf{v}-\frac{\left(\mathbf{v}_r^O\right)^T\mathbf{v}}{\left(\mathbf{v}_r^O\right)^T\mathbf{d}}\mathbf{d}\right]\right)\times\mathbf{v}_r^O\\
&\quad -\mathbf{S}(\boldsymbol{\omega})\,\mathbf{v}_r^O.
\end{aligned} \tag{83}$$

Using Lagrange's formula

$$\mathbf{a}\times(\mathbf{b}\times\mathbf{c}) = (\mathbf{a}\cdot\mathbf{c})\,\mathbf{b}-(\mathbf{a}\cdot\mathbf{b})\,\mathbf{c}\quad\forall_{\mathbf{a},\,\mathbf{b},\,\mathbf{c}\in\mathbb{R}^3}$$

it is possible to rewrite (83) as

$$\begin{aligned}
\dot{\mathbf{v}}_r^O &= -\frac{\|\mathbf{v}_r^O+\mathbf{v}_c\|}{V_d^2\rho}\left(\mathbf{v}_r^O\cdot\mathbf{v}_r^O\right)\left[\mathbf{v}-\frac{\left(\mathbf{v}_r^O\right)^T\mathbf{v}}{\left(\mathbf{v}_r^O\right)^T\mathbf{d}}\mathbf{d}\right]\\
&\quad -\mathbf{S}(\boldsymbol{\omega})\,\mathbf{v}_r^O\\
&= -\mathbf{S}(\boldsymbol{\omega})\,\mathbf{v}_r^O-\frac{\|\mathbf{v}_r^O+\mathbf{v}_c\|}{\rho}\left[\mathbf{v}-\frac{\left(\mathbf{v}_r^O\right)^T\mathbf{v}}{\left(\mathbf{v}_r^O\right)^T\mathbf{d}}\mathbf{d}\right],
\end{aligned} \tag{84}$$

which is identical to (81).

Following the same steps as in Appendix B, the time derivative of the rotation matrix $\mathbf{R}_e$ is given by

$$\dot{\mathbf{R}}_e = \mathbf{S}(\boldsymbol{\omega}_g)\,\mathbf{R}_e,$$

where

$$\boldsymbol{\omega}_g := -\boldsymbol{\omega}+\boldsymbol{\omega}_l,$$

with

$$\boldsymbol{\omega}_l := -\frac{\|\mathbf{v}_r^O+\mathbf{v}_c\|}{V_d^2\rho}\mathbf{v}_r^O\times\left[\mathbf{v}-\frac{\left(\mathbf{v}_r^O\right)^T\mathbf{v}}{\left(\mathbf{v}_r^O\right)^T\mathbf{d}}\mathbf{d}\right].$$

Appendix I
GAS with known ocean currents

The proof of the convergence of the error variables z_1, $\mathbf{z}_3$ and $\mathbf{z}_4$ follows the same steps of Theorem 1 and is therefore omitted. The main difference that results from the presence of known ocean currents is concerned with the proof of the convergence to zero of the sway and heave relative velocities.

When $\mathbf{z}_4$ converges to zero, it is easy to see that $\boldsymbol{\omega}$ converges to $\boldsymbol{\omega}_d$, which is given by

$$\boldsymbol{\omega}_d = \mathbf{K}_2\mathbf{z}_3+\boldsymbol{\omega}_l.$$

Now, as $\mathbf{z}_3$ converges to zero, it follows that $\boldsymbol{\omega}$ converges to $\boldsymbol{\omega}_l$, given in this case by

$$\boldsymbol{\omega}_l = -\frac{\|\mathbf{v}_r^O+\mathbf{v}_c\|}{V_d^2\rho}\mathbf{v}_r^O\times\left[\mathbf{v}-\frac{\left(\mathbf{v}_r^O\right)^T\mathbf{v}}{\left(\mathbf{v}_r^O\right)^T\mathbf{d}}\mathbf{d}\right]. \tag{85}$$

Using the same reasoning as in Theorem 1, it is easily concluded that when $\mathbf{z}$ converges to zero, $\mathbf{R}_e$ converges to an identity matrix. Thus, it follows from (21) that

$$\lim_{\mathbf{z}\to\mathbf{0}}\mathbf{v}_r^O = V_d\begin{bmatrix}1\\0\\0\end{bmatrix} = \mathbf{v}_R. \tag{86}$$

Let $\mathbf{v}_{lr}$ denote the relative lateral velocity of the vehicle, i.e.,

$$\mathbf{v}_{lr} = \begin{bmatrix}0\\v_r\\w_r\end{bmatrix}.$$

Then, the velocity of the vehicle relative to the inertial frame can be written as

$$\mathbf{v} = \begin{bmatrix} u_r \\ 0 \\ 0 \end{bmatrix} + \mathbf{v}_{lr} + \mathbf{v}_c.$$

Now, as when z_1 converges to zero it so happens that u_r convergers to V_d, it can be written

$$\lim_{\mathbf{z}\to\mathbf{0}} \mathbf{v} = \begin{bmatrix} V_d \\ 0 \\ 0 \end{bmatrix} + \mathbf{v}_{lr} + \mathbf{v}_c = \mathbf{v}_R + \mathbf{v}_{lr} + \mathbf{v}_c. \quad (87)$$

Substituting (67), (86), and (87) in (85) and simplifying yields

$$\begin{aligned} \lim_{\mathbf{z}\to\mathbf{0}} \boldsymbol{\omega} &= -\frac{\|\mathbf{v}_R + \mathbf{v}_c\|}{V_d^2 \rho} \mathbf{v}_R \times \mathbf{v}_{lr} \\ &= -\frac{\|\mathbf{v}_R + \mathbf{v}_c\|}{V_d \rho} [1,\, 0,\, 0]^T \times [0,\, v_r,\, w_r] \\ &= \frac{\|\mathbf{v}_R + \mathbf{v}_c\|}{V_d \rho} \begin{bmatrix} 0 \\ w_r \\ -v_r \end{bmatrix}. \end{aligned} \quad (88)$$

Following the same steps as in Theorem 1, the dynamics of the sway and heave relative velocities can now be written as the LTVS

$$\begin{bmatrix} \dot{v}_r \\ \dot{w}_r \end{bmatrix} = \mathbf{A}(t) \begin{bmatrix} v_r \\ w_r \end{bmatrix} + \mathbf{d}(t) \quad (89)$$

driven by a vanishing disturbance, where

$$\mathbf{A}(t) = \begin{bmatrix} -\frac{Y_v + Y_{|v|v}|v_r| - \frac{m_u}{\rho}\|\mathbf{v}_R + \mathbf{v}_c\|}{m_v} & \frac{m_w}{m_v} p \\ -\frac{m_v}{m_w} p & -\frac{Z_w + Z_{|w|w}|w_r| - \frac{m_u}{\rho}\|\mathbf{v}_R + \mathbf{v}_c\|}{m_w} \end{bmatrix}.$$

Since it was assumed that $V_d > V_c$, it follows that

$$\|\mathbf{v}_R + \mathbf{v}_c\| < 2V_d.$$

The reasoning used in Theorem 1 to conclude that the sway and heave velocities converge to zero is now used in conjunction with Assumption (24), which concludes the proof.

Appendix J
Proof of convergence of the sway and heave velocities for non-diagonal mass matrices

This section shows that, for non-diagonal mass matrices

$$\mathbf{M} = \begin{bmatrix} m_{11} & m_{12} & m_{13} \\ m_{12} & m_{22} & m_{23} \\ m_{13} & m_{23} & m_{33} \end{bmatrix},$$

if in addition to the previous assumptions,

$$R_{min} > \max\left(\frac{\max(2m_{12}, m_{12} + m_{13})}{Y_{|v|v}}, \frac{\max(m_{12} + m_{13}, 2m_{13})}{Z_{|w|w}} \right) \quad (90)$$

is satisfied, then the sway and heave velocities still converge to zero in the absence of ocean currents. The proof for the case of constant unknown ocean currents is similar and is therefore omitted.

Notice that, in the proof of Theorem 1, this is the only step that is dependent on the particular structure of the mass matrix. Thus, in the conditions of Theorem 1, it is already known that $\mathbf{z}$ converges to zero, u converges to V_d, and

$$\lim_{\mathbf{z}\to\mathbf{0}} \boldsymbol{\omega} = \frac{1}{\rho} [0, w, -v]^T.$$

Thus, u can $\boldsymbol{\omega}$ can be written as

$$u = V_d + z_1 \quad (91)$$

and

$$\boldsymbol{\omega} = \frac{1}{\rho} [0, w, -v]^T + \boldsymbol{\epsilon}, \quad (92)$$

where z_1 and $\boldsymbol{\epsilon}$ converge to zero.

Let

$$\mathbf{M}_2 = \begin{bmatrix} m_{22} & m_{23} \\ m_{23} & m_{33} \end{bmatrix}, \ \mathbf{M}_{12} = \begin{bmatrix} m_{12} \\ m_{13} \end{bmatrix}, \text{ and } \mathbf{B} = \begin{bmatrix} 1 & 0 \\ 0 & 1 \end{bmatrix}.$$

The dynamics of the sway and heave velocity are given by

$$\mathbf{M}_2 \dot{\mathbf{z}}_5 = -\mathbf{B}\mathbf{S}(\boldsymbol{\omega})\mathbf{M}\mathbf{v} - \mathbf{B}\mathbf{D}_{\mathbf{v}}(\mathbf{v})\mathbf{v} - \dot{u}\mathbf{M}_{12}, \quad (93)$$

where

$$\mathbf{z}_5 = \begin{bmatrix} v \\ w \end{bmatrix}.$$

With the control law (11), $\dot{u} = -k_1 z_1$. Thus, (93) may be rewritten as

$$\mathbf{M}_2 \dot{\mathbf{z}}_5 = -\mathbf{B}\mathbf{S}(\boldsymbol{\omega})\mathbf{M}\mathbf{v} - \mathbf{B}\mathbf{D}_{\mathbf{v}}(\mathbf{v})\mathbf{v} + k_1 z_1 \mathbf{M}_{12}. \quad (94)$$

Consider the Lyapunov-like function

$$V_5 = \frac{1}{2} \mathbf{z}_5^T \mathbf{M}_{12} \mathbf{z}_5.$$

Straightforward computations yield, using (91), (92), and (93),

$$\begin{aligned} \dot{V}_5 = & -\left(Y_v - \frac{m_{11}}{\rho} V_d\right) v^2 - \left(Z_w - \frac{m_{11}}{\rho} V_d\right) w^2 \\ & - \left(Y_{|v|v}|v| - \frac{m_{12}}{\rho} v\right) v^2 + \left(Z_{|w|w}|w| - \frac{m_{13}}{\rho} w\right) w^2 \\ & - \frac{m_{12}}{\rho} w^2 v - \frac{m_{13}}{\rho} v^2 w \\ & - \mathbf{z}_5^T \mathbf{B}\mathbf{S}(\boldsymbol{\epsilon}) \mathbf{M}\mathbf{B}^T \mathbf{z}_5 + \frac{m_{11}}{\rho} z_1 \mathbf{z}_5^T \mathbf{z}_5 \\ & + (z_1 + V_d)\, \mathbf{b}_{\mathbf{v}}{}^T \mathbf{M}\mathbf{S}(\epsilon) \mathbf{B}^T \mathbf{z}_5. \end{aligned} \quad (95)$$

From (95) it is easy to conclude that an upper bound for $\dot{V}_5$ is given by

$$\begin{aligned} \dot{V}_5 \leq & -\left(Y_v - \frac{m_{11}}{R_{min}} V_d\right) v^2 - \left(Z_w - \frac{m_{11}}{R_{min}} V_d\right) w^2 \\ & - \left(Y_{|v|v} - \frac{m_{12}}{R_{min}}\right) |v| v^2 + \left(Z_{|w|w} - \frac{m_{13}}{R_{min}}\right) |w| w^2 \\ & + \frac{m_{12}}{R_{min}} w^2 |v| + \frac{m_{13}}{R_{min}} v^2 |w| \\ & + \left(\sigma_{max}(\mathbf{M}) \|\boldsymbol{\epsilon}\| + \frac{m_{11}}{R_{min}} |z_1|\right) \|\mathbf{z}_5\|^2 \\ & + \left(V_d \sigma_{max}(\mathbf{M}) \|\boldsymbol{\epsilon}\| + \sigma_{max}(\mathbf{M}) |z_1| \|\boldsymbol{\epsilon}\|\right) \|\mathbf{z}_5\|. \end{aligned} \quad (96)$$

Notice that

$$\begin{aligned} \frac{m_{12}}{R_{min}} w^2 |v| + \frac{m_{13}}{R_{min}} v^2 |w| & \leq |v||w| \left(\frac{m_{12}}{R_{min}} |w| + \frac{m_{13}}{R_{min}} |v|\right) \\ & \leq \frac{\max\{m_{12}, m_{13}\}}{R_{min}} \max{}^3 \{|v|, |w|\}. \end{aligned} \quad (97)$$

Using (97) in (96) yields

$$\begin{aligned}\dot{V}_5 \leq & -\left(Y_v - \frac{m_{11}}{R_{min}} V_d\right) v^2 - \left(Z_w - \frac{m_{11}}{R_{min}} V_d\right) w^2 \\ & -\left(Y_{|v|v} - \frac{m_{12}}{R_{min}}\right) |v| v^2 + \left(Z_{|w|w} - \frac{m_{13}}{R_{min}}\right) |w| w^2 \\ & + \frac{\max\{m_{12}, m_{13}\}}{R_{min}} \max{}^3 \{|v|, |w|\} \\ & + \left(\sigma_{max}(\mathbf{M}) \|\boldsymbol{\epsilon}\| + \frac{m_{11}}{R_{min}} |z_1|\right) \|\mathbf{z}_5\|^2 \\ & + \left(V_d \sigma_{max}(\mathbf{M}) \|\boldsymbol{\epsilon}\| + \sigma_{max}(\mathbf{M}) |z_1| \|\boldsymbol{\epsilon}\|\right) \|\mathbf{z}_5\| . \end{aligned} \tag{98}$$

Under Assumptions (14) and (90), it is possible to rewrite (98) as

$$\begin{aligned}\dot{V}_5 \leq & -C_v v^2 - C_w w^2 - C_{|v|v} |v|^3 - C_{|w|w} |w|^3 \\ & + \left(\sigma_{max}(\mathbf{M}) \|\boldsymbol{\epsilon}\| + \frac{m_{11}}{R_{min}} |z_1|\right) \|\mathbf{z}_5\|^2 \\ & + \left(V_d \sigma_{max}(\mathbf{M}) \|\boldsymbol{\epsilon}\| + \sigma_{max}(\mathbf{M}) |z_1| \|\boldsymbol{\epsilon}\|\right) \|\mathbf{z}_5\| , \end{aligned} \tag{99}$$

where

$$\begin{aligned} C_v &:= Y_v - \frac{m_{11}}{R_{min}} V_d > 0, \\ C_w &:= Z_w - \frac{m_{11}}{R_{min}} V_d > 0, \\ C_{|v|v} &:= Y_{|v|v} - \frac{m_{12}}{R_{min}} - \frac{\max\{m_{12}, m_{13}\}}{R_{min}} > 0, \\ C_{|w|w} &:= Z_{|w|w} - \frac{m_{13}}{R_{min}} - \frac{\max\{m_{12}, m_{13}\}}{R_{min}} > 0. \end{aligned}$$

Let $C_1 := \min\{C_v, C_w\}$, $C_2 := \min\{C_{|v|v}, C_{|w|w}\}$, $C_3 := \max\left\{\sigma_{max}(\mathbf{M}), \frac{m_{11}}{R_{min}}\right\}$, $C_4 := V_d \sigma_{max}(\mathbf{M})$, $C_5 := \sigma_{max}(\mathbf{M})$, and

$$\mathbf{u}_l = \begin{bmatrix} z_1 \\ \boldsymbol{\epsilon} \end{bmatrix}.$$

Then,

$$\begin{aligned}\dot{V}_5 \leq & -C_1 \|\mathbf{z}_5\|^2 - C_2 \left(|v|^3 + |w|^3\right) \\ & + C_3 \|\mathbf{u}_l\| \|\mathbf{z}_5\|^2 + \left(C_4 \|\mathbf{u}_l\| + C_5 \|\mathbf{u}_l\|^2\right) \|\mathbf{z}_5\| \end{aligned} \tag{100}$$

is an upper bound for (99). Let $0 < \gamma < 1$. Then, it is possible to rewrite (100) as

$$\begin{aligned}\dot{V}_5 \leq & -C_1 (1-\gamma) \|\mathbf{z}_5\|^2 \\ & -\gamma C_1 \|\mathbf{z}_5\|^2 - C_2 \left(|v|^3 + |w|^3\right) + C_3 \|\mathbf{u}_l\| \|\mathbf{z}_5\|^2 \\ & + \left(C_4 \|\mathbf{u}_l\| + C_5 \|\mathbf{u}_l\|^2\right) \|\mathbf{z}_5\| . \end{aligned} \tag{101}$$

Now, using $\|\mathbf{z}_5\| \leq \sqrt{2} \|\mathbf{z}_5\|_\infty$ and $\|\mathbf{u}_l\| \leq 2 \|\mathbf{u}_l\|_\infty$ it is possible to further write, from (101),

$$\begin{aligned}\dot{V}_5 \leq & -C_1 (1-\gamma) \|\mathbf{z}_5\|^2 \\ & -\gamma C_1 \|\mathbf{z}_5\|^2 - C_2 \left(|v|^3 + |w|^3\right) \\ & + 4 C_3 \|\mathbf{u}_l\|_\infty \|\mathbf{z}_5\|_\infty^2 \\ & + \left(2\sqrt{2} C_4 \|\mathbf{u}_l\|_\infty + 4\sqrt{2} C_5 \|\mathbf{u}_l\|^2\right) \|\mathbf{z}_5\|_\infty . \end{aligned} \tag{102}$$

Now, notice that (102) can be rewritten as

$$\begin{aligned}\dot{V}_5 \leq & -C_1 (1-\gamma) \|\mathbf{z}_5\|^2 \\ & -\gamma C_1 \|\mathbf{z}_5\|_\infty \left[\|\mathbf{z}_5\|_\infty - \left(\frac{2\sqrt{2} C_4}{\gamma C_1} \|\mathbf{u}_l\|_\infty + \frac{4\sqrt{2} C_5}{\gamma C_1} \|\mathbf{u}_l\|^2\right)\right] \\ & -C_2 \|\mathbf{z}_5\|_\infty^2 \left(\|\mathbf{z}_5\|_\infty - \frac{4 C_3}{C_2} \|\mathbf{u}_l\|_\infty\right), \end{aligned} \tag{103}$$

from which follows that

$$\dot{V}_5 \leq -C_1 (1-\gamma) \|\mathbf{z}_5\|^2 \, \forall_{\|\mathbf{z}_5\|_\infty > s\left(\|\mathbf{u}_l\|_\infty\right)}, \tag{104}$$

where

$$s\left(\|\mathbf{u}_l\|_\infty\right) = \max\left\{\frac{4 C_3}{C_2}, \left(\frac{2\sqrt{2} C_4}{\gamma C_1} + \frac{4\sqrt{2} C_5}{\gamma C_1} \|\mathbf{u}_l\|\right)\right\} \|\mathbf{u}_l\|_\infty$$

is a class $\mathcal{K}$ function. Since, in addition to (104), V_5 satisfies

$$\frac{1}{2} \sigma_{min}(\mathbf{M}_2) \|\mathbf{z}_5\|_\infty^2 \leq V_5 \leq \sigma_{max}(\mathbf{M}_2) \|\mathbf{z}_5\|_\infty^2 ,$$

it follows that the dynamic system (94) is ISS with $\mathbf{u}_l$ as input. Since $\mathbf{u}_l$ converges to zero, it follows that so do the sway and heave velocities.

Pedro Batista received, in 2005, the Licenciatura degree in Electrical and Computer Engeneering from Instituto Superio Técnico (IST), Lisbon, Portugal, where he is currently pursuing the Ph.D. degree in the same field.

From 2004 to 2006 he was Monitor in the Department of Mathematics of IST and he has also received the Diploma de Mérito twice during his graduation. His research interests include sensor-based control and estimation of autonomous vehicles.

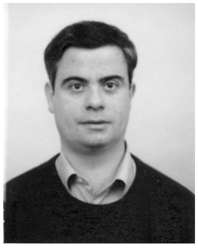

Carlos Silvestre received the Licenciatura degree in Electrical Engineering from the Instituto Superior Técnico (IST) of Lisbon, Portugal, in 1987 and the M.Sc. degree in Electrical Engineering and the Ph.D. degree in Control Science from the same school in 1991 and 2000, respectively. Since 2000, he is with the Department of Electrical Engineering of Instituto Superior Técnico, where he is currently an Assistant Professor of Control and Robotics. Over the past years, he has conducted research on the subjects of vehicle and mission control of air and underwater robots. His research interests include linear and nonlinear control theory, coordinated control of multiple vehicles, gain scheduled control, integrated design of guidance and control systems, inertial navigation systems, and mission control and real time architectures for complex autonomous systems with applications to unmanned air and underwater vehicles.

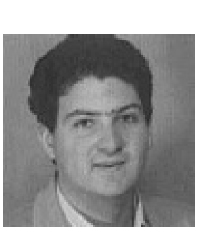

Paulo Oliveira completed the Ph.D. in 2002 from the Instituto Superior Técnico, Lisbon, Portugal. He is an Assistant Professor at the Department of Electrical Engineering and Computer Science of the Instituto Superior Técnico, Lisbon, Portugal and researcher in the Institute for Systems and Robotics, Lisbon, Portugal. The areas of scientific activity are Robotics and Autonomous Vehicles with special focus on the fields of Estimation, Sensor Fusion, Navigation, Positioning, and Signal Processing. He participated in more than 10 Portuguese and European Research projects, in the last 20 years.